Physica D 241 (2012) 2042–2057

Contents lists available at SciVerse ScienceDirect

Physica D

journal homepage: www.elsevier.com/locate/physd

Nonsmooth dynamics in spiking neuron models

S. Coombes *, R. Thul, K.C.A. Wedgwood

School of Mathematical Sciences, University of Nottingham, Nottingham, NG7 2RD, UK

ARTICLE INFO

Article history:
Available online 13 May 2011

Keywords:
Integrate-and-fire
Spiking neuron model
Nonsmooth bifurcation
Linear-coupling

ABSTRACT

Large scale studies of spiking neural networks are a key part of modern approaches to understanding the dynamics of biological neural tissue. One approach in computational neuroscience has been to consider the detailed electrophysiological properties of neurons and build vast computational compartmental models. An alternative has been to develop minimal models of spiking neurons with a reduction in the dimensionality of both parameter and variable space that facilitates more effective simulation studies. In this latter case the single neuron model of choice is often a variant of the classic integrate-and-fire model, which is described by a nonsmooth dynamical system. In this paper we review some of the more popular spiking models of this class and describe the types of spiking pattern that they can generate (ranging from tonic to burst firing). We show that a number of techniques originally developed for the study of impact oscillators are directly relevant to their analysis, particularly those for treating grazing bifurcations. Importantly we highlight one particular single neuron model, capable of generating realistic spike trains, that is both computationally cheap and analytically tractable. This is a planar nonlinear integrate-and-fire model with a piecewise linear vector field and a state dependent reset upon spiking. We call this the PWL-IF model and analyse it at both the single neuron and network level. The techniques and terminology of nonsmooth dynamical systems are used to flesh out the bifurcation structure of the single neuron model, as well as to develop the notion of Lyapunov exponents. We also show how to construct the phase response curve for this system, emphasising that techniques in mathematical neuroscience may also translate back to the field of nonsmooth dynamical systems. The stability of periodic spiking orbits is assessed using a linear stability analysis of spiking times. At the network level we consider linear coupling between voltage variables, as would occur in neurobiological networks with gap-junction coupling, and show how to analyse the properties (existence and stability) of both the asynchronous and synchronous states. In the former case we use a phase-density technique that is valid for any large system of globally coupled limit cycle oscillators, whilst in the latter we develop a novel technique that can handle the nonsmooth reset of the model upon spiking. Finally we discuss other aspects of neuroscience modelling that may benefit from further translation of ideas from the growing body of knowledge on nonsmooth dynamics.

1. Introduction

Spiking neurons are at the heart of many computational models of the brain that aim to improve our understanding of brain function and dysfunction. The Blue Brain Project [1] is a case in point. This has utilised IBM's Blue Gene parallel supercomputer to attempt the construction of a biologically accurate model of neural tissue from first principles. At present initial simulations of $\sim 10^4$ biophysically detailed neurons have been performed, setting the scale of the tissue at roughly one neocortical column. Given that a whole human brain contains 10^{10} neurons there has been a push in the computational neuroscience community to develop complimentary models that are reduced in their complexity yet still able to generate the rich repertoire of behaviour seen in a real nervous system. Perhaps the most famous example of such a model is the FitzHugh–Nagumo model [2], comprising two coupled ordinary differential equations for the generation of continuous action potential like shapes of spiking voltage activity. In this case analytical progress has also been possible with one further step, namely, the introduction of piecewise linear (PWL) nullclines. This gives rise to the so-called McKean model [3], for which a number of results about the existence and stability of periodic orbits are now known [4–6]. Indeed there are now a number of planar PWL single neuron models for mimicking the behaviour of tonically firing neurons, and we refer the reader to [7] for a recent discussion. Moreover, the PWL nature of such models means that

* Corresponding author. Tel.: +44 115 846 7836; fax: +44 115 951 4951.
E-mail addresses: stephen.coombes@nottingham.ac.uk (S. Coombes), ruediger.thul@nottingham.ac.uk (R. Thul), pmxkw2@nottingham.ac.uk (K.C.A. Wedgwood).

0167-2789/
doi:10.1016/j.physd.2011.05.012

techniques from nonsmooth dynamics are particularly relevant to their analysis, and indeed recent progress on understanding canard explosions has been made by studying PWL models of FitzHugh–Nagumo type [8]. However, the spiking patterns of such planar models are typically not as diverse as one needs to mimic realistic firing patterns, such as bursting.

The currently most successful class of minimal models that satisfy the criterion of being able to generate realistic firing patterns are those of the integrate-and-fire (IF) type, where a simple threshold unit is used to caricature the excitable aspect of real cells that gives rise to an action potential spike. In these models the spike shape is discontinuous. Recent work by Izhikevich has developed a large-scale thalamo-cortical model with $\sim 10^6$ neurons using a phenomenological two dimensional nonlinear IF model [9]. One key aspect of any IF model is the discontinuous reset of a state variable upon reaching some threshold for spiking. It is this particular harsh nonlinearity in the dynamics that endows these models with interesting dynamics and precludes their description using the machinery of smooth dynamical systems. Indeed they have much in common with models of impacting systems that have been developed for the study of mechanical structures such as rocking blocks [10], rattling gear boxes [11] and print hammers [12]. For a discussion of impacting systems in general we refer the reader to the recent book by di Bernardo et al. [13]. Thus it is timely to revisit the dynamics of IF models using the techniques developed for the study of more general nonsmooth systems, such as those reviewed in [14], and develop the mathematical insight into network behaviour that can complement simulation studies that are being performed in the computational neuroscience community.

In Section 2 we provide a review of some of the more popular models of IF type that are currently being used as models of spiking neurons. To illustrate that nonsmooth bifurcations play a fundamental role in the description of their behaviour we present an analysis of the periodically forced leaky IF model in Section 3. Here we show that grazing bifurcations are especially important in determining the Arnol'd tongue diagram for mode-locked responses, and note the relevance of this to modelling spike trains in the sensory periphery. For modelling the spike trains in deeper brain regions, such as the cortex, we introduce a new class of IF model in Section 4. This model is able to reproduce a range of spiking patterns, from tonic to burst firing, yet is analytically tractable. In essence the model below the threshold for firing evolves according to a planar PWL dynamical system. We present an original bifurcation analysis of this model in response to constant current injection focusing on local discontinuity induced bifurcations. Next in Section 5 we show how to construct periodic orbits and determine their stability as well as calculate the phase response curve (by adapting techniques originally developed for the analysis of limit cycles in smooth dynamical systems). In Section 6 spike-adding bifurcations (for bursting orbits) are described in terms of bifurcations of an associated one-dimensional return map. The notion of Lyapunov exponents is developed in Section 7, using techniques originally developed for the analysis of impact oscillators. Next in Section 8 we turn to the construction and analysis of neural networks. We focus on gap-junction coupling, where the natural way to describe electrically interacting cells is via an ohmic resistance, which translates into a linear coupling between voltage state variables. For large globally coupled networks we show how to determine the properties of the synchronous and asynchronous states (existence and stability). Finally we end with a discussion of future challenges in the understanding of neurodynamical systems that are likely to benefit from further cross-over of ideas from nonsmooth dynamical systems.

2. A review of integrate-and-fire models

Although conductance-based models like that of Hodgkin and Huxley [15] provide a level of detail that helps us to understand how neural cells generate action-potential electrical spikes, their high dimensionality (four for Hodgkin–Huxley though rising to hundreds for compartmental models that express realistic ionic currents) precludes them from detailed study, especially at the network level. Thus simpler models are more appealing, especially if they can be fitted to single neuron data. It is now known that nonlinear extensions of the basic leaky IF model can accurately fit intracellular voltage recordings [16]. A one-dimensional nonlinear IF model takes the form

$$\frac{dv}{dt} = f(v) + I(t), \tag{1}$$

such that v is reset to v_R just after reaching the threshold value $v_{th} > v_R$. Here v is interpreted as a voltage variable and $I(t)$ is an external drive (that might be under the control of an experimentalist or arise from the activity of other neurons to which a cell is coupled). Firing times are defined iteratively according to

$$T_n = \inf\{t | v(t) \geq v_{th};\ t \geq T_{n-1}\}. \tag{2}$$

One-dimensional IF models with a fixed voltage threshold are caricatures of excitable neural systems and as such it is worth mentioning that they cannot adequately capture the refractory properties of real neurons. This is often achieved with the introduction of an absolute time during which they cannot fire after reaching the threshold or by the introduction of a time dependent threshold that increases after a firing event and makes it harder for the neuron to subsequently fire (mimicking a relative refractory period), as reviewed in [17]. Moreover, real neurons (and Hodgkin–Huxley style models) do not possess a fixed voltage threshold, and firing ultimately depends on the state of receptors within a membrane. Although differential equations for the threshold in IF models can be found that mimic more closely the properties of real neurons [18], we limit our discussion in this paper to models with a constant threshold.

2.1. Leaky IF model

The leaky IF model (LIF) is attributed to Lapicque in 1907, although the phrase "integrate-and-fire" was first coined by Bruce Knight in the 1960s [19]. It is defined by (1) and (2) with the choice

$$f(v) = -\frac{v}{\tau}, \quad \tau > 0. \tag{3}$$

Because of its linear nature we may solve the sub-threshold dynamics of the model exactly for $v < v_{th}$ with initial data $v(t_0) < v_{th}$ at time $t = t_0$ (using an integrating factor, variation of constants or Green's function):

$$v(t) = v(t_0)e^{-(t-t_0)/\tau} + \int_{t_0}^{t} e^{-(t-s)/\tau} I(s)ds. \tag{4}$$

For a periodic input the system may well respond periodically though without reaching the threshold. This is commonly referred to as a sub-threshold oscillation and is to be distinguished from the case when oscillations arise via the reset mechanism. Consider in particular the case of a constant drive, where the threshold can only be reached from $v(t_0)$ if $I\tau > v_{th}$. The threshold will subsequently be reached from v_R and a periodic oscillation will occur. The period of oscillation $\Delta = T_{n+1} - T_n$ is determined by setting $v(T_{n+1}) = v_{th}$ with $v(T_n) = v_R$, giving

$$\Delta = \tau \ln\left(\frac{I\tau - v_R}{I\tau - v_{th}}\right) H(I\tau - v_{th}), \tag{5}$$

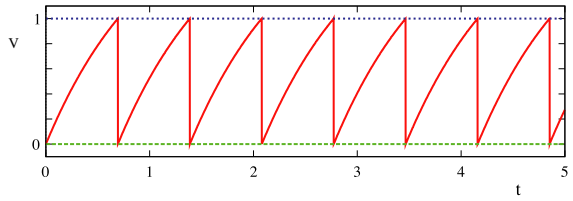

Fig. 1. Voltage trace for an LIF oscillator with constant drive $I = 2$ with $\tau = 1$, $v_{\rm th} = 1$ and $v_{\rm R} = 0$.

where H is the Heaviside step function. The inclusion of the Heaviside term reflects the fact that oscillations do not occur for $I\tau < v_{\rm th}$. Electrophysiologists often classify neuron response in terms of the so-called $f - I$ curve, which shows the frequency of oscillation as a function of the time independent drive I. For the LIF model this is easily constructed from (5) using $f = \Delta^{-1}$, showing a sharp rise in f (from zero) as I increases through the critical value $v_{\rm th}/\tau$. A plot of the response of the LIF model to constant drive I is shown in Fig. 1. Here one sees that the model does not capture the essential shape of a real action potential. Rather the IF model is deemed to be good at capturing the time of generation of an action potential. Since many models of synaptic (chemical) interaction are based on spike-times, rather than spike shapes, this favours the IF model in large scale simulations of synaptically coupled neurons. The tractability of this single neuron model (linear dynamics between firing events) means that it is particularly suited to analysis at the network level with event based models of chemical synapses. Indeed a theory of phase-locked behaviour for strong coupling has been developed for just this scenario [20]. However, gap junction (linear) coupling between neurons means that the action potential shape is communicated from one neuron to another and so LIF models are (without modification) poor candidates for use in this case.

2.2. Nonlinear IF models

The quadratic IF (QIF) neuron is the simplest generalisation of the LIF model that captures qualitatively the behaviour of the $f - I$ curve of a large family of more realistic models [21]. Interestingly, this model was apparently already known to Alan Hodgkin, and used to fit some of his data (and also subsequently analysed by Bruce Knight). Up to shifts and constant factors it is defined by

$$f(v) = v^2. \tag{6}$$

Unlike the LIF model the QIF does allow a representation of an action potential shape (for $I > 0$ the voltage rises sharply to threshold), as shown in Fig. 2. For $I < 0$ there are two equilibria (one stable and the other unstable) and for $I > 0$ these disappear via a saddle–node bifurcation at $I = 0$. In the oscillatory regime ($I > 0$) the trajectory (for constant drive) can be integrated for $T_n < t < T_{n+1}$ to give

$$v(t) = \sqrt{I}\tan\left(\tan^{-1}\left(\frac{v_{\rm R}}{\sqrt{I}}\right) + \sqrt{I}(t - T_n)\right). \tag{7}$$

The period of oscillation is calculated by setting $v(T_{n+1}) = v_{\rm th}$ with $v(T_n) = v_{\rm R}$ giving

$$\Delta = \frac{1}{\sqrt{I}}\left(\tan^{-1}\left(\frac{v_{\rm th}}{\sqrt{I}}\right) - \tan^{-1}\left(\frac{v_{\rm R}}{\sqrt{I}}\right)\right) H(I).$$

In the limit $v_{\rm th} \to \infty$ and $v_{\rm R} \to -\infty$ we see that $\Delta = \pi/\sqrt{I}$ (and we have blowup of the voltage trajectory in finite time), and the $f - I$ curve shows a $\sqrt{I}$ dependence, which matches many cortical neurons much better than the LIF $f - I$ curve. For a further discussion of this model we refer the reader to the book by Izhikevich [22].

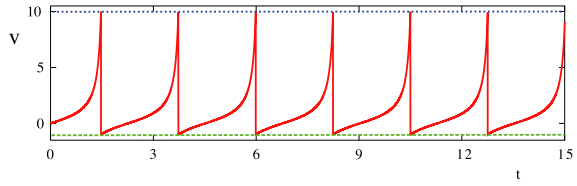

Fig. 2. Voltage trace for the QIF oscillator with constant drive $I = 1$ with $v_{\rm th} = 10$ and $v_{\rm R} = -1$.

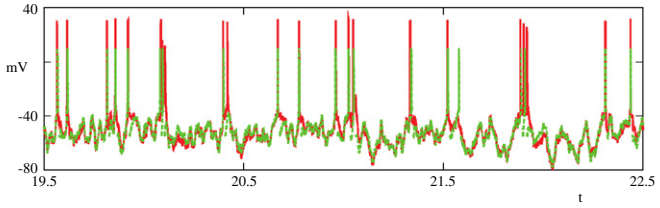

Fig. 3. Sample voltage traces (mV) as a function of time (s) from the linear-exponential IF model (green dashed line) and data (red solid line) from a layer-5 pyramidal cell in response to a noisy current injection (constructed from two summed Ornstein–Uhlenbeck processes, see [16] for further details). (For interpretation of the references to colour in this figure legend, the reader is referred to the web version of this article.)

With the improvement in neuronal modelling by simply changing the shape of the nonlinearity from (3) to (6) this raises the question as to whether more judicious choices can improve things further still. Interestingly Fourcaud–Trocmé et al. [23] have shown that choosing $f(v) = \exp(v)$ (up to shifts and scaling) can act as an approximation of a more detailed conductance-based spiking model. In fact it has now been shown that real cortical data (from layer-5 pyramidal cells) can be very accurately fitted with the following choice [16]:

$$f(v) = -\frac{1}{\tau}(v - v_{\rm L}) + \frac{\kappa}{\tau}e^{(v - v_\kappa)/\kappa}, \tag{8}$$

with $v_{\rm th} = 30.0$, $v_{\rm R} = -71.2$, $v_{\rm L} = -68.5$, $\tau = 3.3$, $v_\kappa = -61.5$ and $\kappa = 4$. Fig. 3 nicely illustrates the strong fit of the model to real data for a stimulation protocol which is a noisy current injection. Similarly to the QIF model the linear-exponential IF (LEIF) model obtained using (8) has two equilibria (defined by $f(v) + I = 0$) which disappear in a saddle–node bifurcation when $I = -f(v^*)$, where v^* is defined by $f'(v^*) = 0$. In common with the QIF model it is able to support oscillations with arbitrarily low frequency just beyond the bifurcation point. Both the QIF and LEIF models have only a weak dependence on the choice of threshold value since they both blow up in finite time (in the absence of a threshold).

2.3. Planar IF models

Unfortunately, one dimensional nonlinear IF models, as they stand, are unable to reproduce bursting patterns of activity, which are typically associated with slow calcium dependent processes. One way to incorporate such a slow process is by coupling the voltage dynamics to a *recovery* or *adaptive* process in the following manner:

$$\frac{{\rm d}v}{{\rm d}t} = f(v) - a + I, \qquad \frac{1}{\omega}\frac{{\rm d}a}{{\rm d}t} = \beta v - a. \tag{9}$$

Here the parameters β and ω, respectively, describe the sensitivity and decay rate of the adaptive process. Upon reaching the threshold the voltage is reset ($v \to v_{\rm R}$) and a is adjusted according to $a \to a + k$. The Izhikevich model [24,25] is one such model with $f(v) = 0.04v^2 + 5v + 140$. Interestingly this model can capture a number of neuronal firing patterns including tonic (repetitive) spiking, bursting and fast spiking as illustrated in Fig. 4, despite

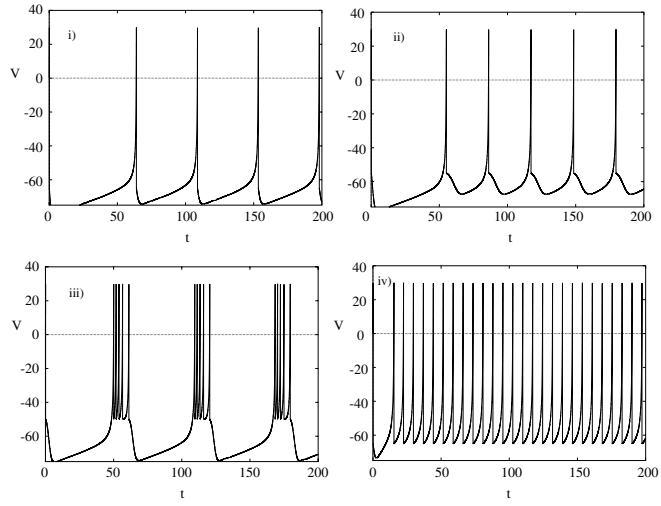

Fig. 4. Firing patterns in the Izhikevich model with $I = 10$ and $v_{\rm th} = 30$. Voltage traces as a function of time for (i) tonic spiking ($\alpha = 0.02$, $\beta = 0.2$, $v_{\rm R} = -65$, $k = 8$), (ii) tonic spiking ($\alpha = 0.02$, $\beta = 0.2$, $v_{\rm R} = -55$, $k = 4$), (iii) bursting ($\alpha = 0.02$, $\beta = 0.2$, $v_{\rm R} = -50$, $k = 2$), and (iv) fast spiking ($\alpha = 0.1$, $\beta = 0.2$, $v_{\rm R} = -65$, $k = 2$).

its sensitivity to the choice of threshold value [26]. It is worth noting that a similar model to that of Izhikevich was independently introduced by Gröbler et al. [27] as a model of a pyramidal cell in hippocampus CA3. The adaptive exponential integrate-and-fire model is obtained using a linear-exponential term for $f(v)$ (as in Eq. (8)) [28,29], whilst the quartic model is obtained by choosing $f(v) = v^4 + 2\omega v$ [30]. Both are able to produce a wide variety of firing patterns, and the quartic model in particular has a very nice repertoire of responses ranging from tonic spiking to bursting as well supporting phasic responses, rebound, spike frequency adaptation, sub-threshold oscillations and much more, all of which are discussed in detail in [30].

Apart from the LIF model none of the models described above admits to closed form solutions for arbitrary (non-constant) drive. A somewhat overlooked tractable (one dimensional) nonlinear IF model is that of Karbowski and Kopell [31], with a nonlinearity given by $f(v) = |v|$, which we shall call the absolute IF model (AIF). Because of the choice of a PWL form of the nonlinearity the AIF model can be explicitly analysed. Moreover, it is also capable of generating behaviour consistent with that of a fast-spiking interneuron [32]. The generalisation of the model to allow for bursting behaviour is easily achieved by extending it to the form of (9). A minimal AIF model with adaptation is obtained for $f(v) = |v|$ and $\beta = 0$. For sufficiently small k the model fires tonically and for larger values of k the model can also fire in a burst mode. The mechanism for this behavior in the AIF model (and indeed all planar models discussed here) is most easily understood in reference to the geometry of the phase-plane. We illustrate, in Fig. 5, the phase plane for the AIF model, and refer the reader to [32] for a more detailed discussion and analysis of this model. The analysis of how parameter space partitions into tonic, 1-spike per burst, 2-spike per burst, etc. firing patterns is an open mathematical (classification) challenge. It is worth noting that all the planar models considered here have much in common and can generate a very similar repertoire of firing behaviours, though the AIF model does not have trajectories that blow up in finite time (in the absence of a threshold).

3. Bifurcations of the periodically forced LIF neuron

Because all IF models include a threshold process spikes can be created or annihilated as a voltage trajectory tangentially

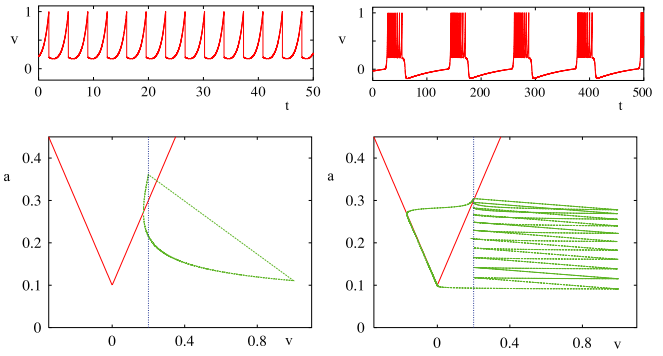

Fig. 5. Top left: Tonic firing in the AIF model with spike adaptation. Here $\omega = 1/3$ and $k = 0.75\omega$. Top right: Burst firing in the AIF model with spike adaptation. Here $\omega = 1/75$ and $k = 2\omega$. Bottom left: A periodic orbit in the (v, a) plane corresponding to the tonic spiking trajectory shown above (green curve). Also shown is the voltage nullcline (red lines) as well as the value of the reset (blue dashed line). Bottom right: Burst firing in the AIF model with spike adaptation. Here $\omega = 1/75$, and $k = 2\omega$. Other parameters are $v_{\rm R} = 0.2$, $v_{\rm th} = 1$ and $I = 0.1$. (For interpretation of the references to colour in this figure legend, the reader is referred to the web version of this article.)

intersects the threshold. This is naturally the case when a time-varying current injection (such as a periodically varying synaptic current) is considered (and not just a constant drive). Thus it becomes important not only to assess the stability of spike trains to perturbations that leave the number of spikes unchanged (though do modify firing times), but to address any instabilities that may arise via nonsmooth grazing bifurcations. To show how this can be done we present an analysis of the periodically forced LIF model, though stress that the ideas we present here carry over to more complicated IF models such as those reviewed in Section 2.

The phenomenon of mode-locking is well documented in the literature on the periodic forcing of nonlinear oscillators. It is most commonly studied in the context of the standard circle map (see for example [33]). This map is known to support regions of parameter space where the rotation number (average rotation per map iterate) takes the value p/q, where $p, q \in \mathbb{Z}^+$. These regions are referred to as $p : q$ Arnol'd tongues. In a neural context mode-locked solutions are simply identically recurring firing patterns for which a neuron fires p spikes for every q cycles of forcing. With an increase of the coupling amplitude from zero, Arnol'd tongues in the standard circle map typically open as a wedge, centered at points in parameter space where the natural frequency of the oscillator is rational. In between tongues, quasi-periodic behaviour emanating from irrational points on the amplitude/frequency axis, is observed. The technique for calculating such tongues in IF models was first developed by Keener et al. [34] and later expanded upon in [35,36].

Consider a LIF neuron with threshold at $v_{\rm th} = 1$ and reset level $v_{\rm R} = 0$ being driven by a Δ periodic signal $I(t) = I(t + \Delta)$. An implicit map of the firing times may be obtained by integrating between reset and threshold according to Eq. (4). Introducing the function

$$G(t) = \int_{-\infty}^{0} {\rm e}^{s/\tau} I(t+s)\,{\rm d}s, \qquad G(t) = G(t+\Delta), \tag{10}$$

gives

$${\rm e}^{T_{n+1}/\tau}[G(T_{n+1}) - 1] = {\rm e}^{T_n/\tau} G(T_n). \tag{11}$$

Defining

$$F(t) = {\rm e}^{t/\tau}[G(t) - 1], \tag{12}$$

we obtain an implicit map of the firing times in the form

$$F(T_{n+1}) = F(T_n) + {\rm e}^{T_n/\tau}. \tag{13}$$

A 1:1 mode-locked solution is defined by $T_n = (n+\phi)\Delta$, with $\phi \in [0, 1)$, giving a fixed point equation

$$G(\phi\Delta) = \frac{1}{1-\mathrm{e}^{-\Delta/\tau}}. \tag{14}$$

Stability is examined by considering perturbations of the form $T_n \to T_n + \delta_n$, giving

$$\delta_{n+1} = \kappa(\phi)\delta_n, \qquad \kappa(\phi) = \mathrm{e}^{-\Delta/\tau}\frac{I(\phi\Delta)}{I(\phi\Delta)-1/\tau}. \tag{15}$$

Solutions are stable if $|\kappa(\phi)| < 1$. The borders of the regions where 1:1 solutions become unstable are defined by $\kappa(\phi) = 1$ (tangent bifurcation) and $\kappa(\phi) = -1$ (period doubling bifurcation). However, solutions may also lose stability in a nonsmooth fashion in two possible ways, which we shall refer to as type (a) and type (b). In type (a) there is a tangential intersection of the trajectory with the threshold value such that upon variation of the bifurcation parameter the local maxima of the voltage trajectory passes through threshold from above. This is defined by $\dot v = -v/\tau + I = 0$, so that $I(T_n) = 1/\tau$ or equivalently $F'(T_n) = 0$. In type (b) a sub-threshold local maxima increases through threshold leading to the creation of a new firing event at some earlier time than usual. This is defined by $F(T^*) = F(T_n) + \mathrm{e}^{T_n/\tau}$ and $F'(T^*) = 0$ with $T^* < T_{n+1}$ and T_{n+1} is the solution to $F(T_{n+1}) = F(T_n) + \mathrm{e}^{T_n/\tau}$.

As an example consider the choice

$$I(t) = I_0 + \begin{cases} +\epsilon & 0 \le t < \Delta/2 \\ -\epsilon & \Delta/2 < t < \Delta \end{cases}. \tag{16}$$

In this case the condition $|\kappa(\phi)| = 1$ is independent of ϕ, since $I(\phi) = I_0 \pm \epsilon$. A tangent bifurcation occurs when $\kappa = 1$:

$$\pm\epsilon = -I_0 + \frac{1/\tau}{1-\mathrm{e}^{-\Delta/\tau}}. \tag{17}$$

A nonsmooth bifurcation of type (b) is defined by the two equations

$$\tau(I+\epsilon)(1-\mathrm{e}^{-\Delta(1/2-\phi)/\tau}) = 1 \tag{18}$$

$$\overline{v}\mathrm{e}^{-\phi\Delta/\tau} + \tau(I+\epsilon)(1-\mathrm{e}^{-\phi\Delta/\tau}) = 1, \tag{19}$$

where $0 < \phi < 1/2$ and

$$\overline{v} = \mathrm{e}^{-\Delta/2\tau} + \tau(I-\epsilon)(1-\mathrm{e}^{-\Delta/2\tau}). \tag{20}$$

Between them the above two bifurcations define the 1:1 Arnol'd tongue as shown in Fig. 6 (left) (period doubling and type (a) bifurcations are not possible for the parameter values shown). The construction of other tongues with more general values of $p : q$ is carried out in [35,36], and the resultant tongue structure calculated for $I(t) = I_0 + \epsilon\sin 2\pi t$ is shown in Fig. 6 (right). Once again the right hand borders of Arnol'd tongues are defined by type (b) nonsmooth bifurcations (and all others by tangent bifurcations of the firing map).

In a pair of recent papers [37,38] it has been shown that spike data from stellate cells in the ventral cochlear nucleus are very well explained by a LIF model with threshold noise, and that Arnol'd tongues are a practical way to understand the way in which single cells in the auditory periphery encode periodic stimuli. Indeed, responses of LIF models to chaotic forcing have also been shown to be largely determined by grazing bifurcations [39]. The techniques described above have also been applied to several variants of the LIF model, including the IF-or-burst model [40], the "ghostburster" model [41] and the resonate-and-fire neuron model [42] as well as to PWL neuron models [43]. Most recently an IF model with a slow T-type calcium current has been studied and been shown to support chaotic behaviour in response to periodic forcing [44]. Interestingly by determining the condition for a grazing bifurcation it was shown that knowledge of unstable periodic orbits (existence and stability) could be combined with the grazing condition to determine an effective one-dimensional map that captured the essentials of the chaotic behavior. This map is discontinuous and has strong similarities with the universal limit mapping in grazing bifurcations derived in the context of impacting mechanical systems [45]. This latter map was derived for grazing bifurcations that occur in impacting mechanical oscillators and can support period adding cascades with or without chaotic bands.

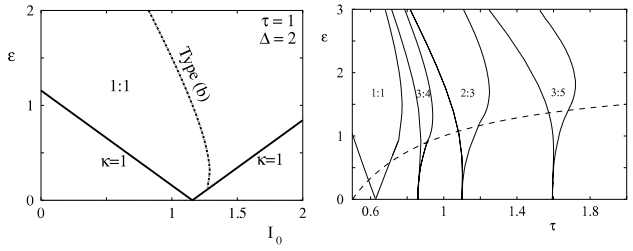

Fig. 6. Left: 1:1 Arnol'd tongue in the LIF model with $I(t)$ a Δ-periodic square wave with amplitude $I_0 \pm \epsilon$. Note that a type (b) nonsmooth bifurcation significantly shapes the tongue structure. Here $\tau = 1$ and $\Delta = 2$. Right: $p : q$ Arnol'd tongues in the LIF model with $I(t) = I_0 + \epsilon\sin 2\pi t$. Here $I_0 = 2$. Below the dashed line the firing map is invertible.

4. A piecewise linear IF model

The aspect of the LIF model that allows one to perform an analysis such as the one above is obviously its linearity (below threshold). A similar analysis for say the QIF, LEIF or Izhikevich model would be much harder owing to the inherent nonlinear nature of these models. However, the AIF model described in Section 2 is a natural starting point for the development of a more general PWL spiking neuron model that can be explicitly analysed. The use of PWL modelling is already quite common in neuroscience, with the McKean model [3] being a classic example. This may be regarded as a variant of the FitzHugh–Nagumo model [2] that provides a planar model of an excitable cell in which the dynamics is broken into simpler linear pieces. An extension of this approach to develop PWL caricatures of other single neuron models, including the Morris–Lecar model, has recently been pursued by Tonnelier and Gerstner [46] and Coombes [7].

In this section we advocate a new type of PWL IF model, that we shall call the PWL-IF model. It is a generalisation of the AIF model with adaptation that we write in the form of (9) with

$$f(v) = \begin{cases} v & v \ge 0 \\ -sv & v < 0. \end{cases} \tag{21}$$

For a constant drive I the model may exhibit a number of different periodic attractors, and in particular we distinguish between those that remain sub-threshold, and those that cross threshold, which we shall term *spiking solutions*. We make further distinctions between spiking solutions as follows.

Fast spiking orbits: Attracting limit cycles which have $v > 0$ along the entire orbit and which have $v(t^*) = v_{\rm th}$ at precisely one value of $t^* \in [t, t+\Delta]\ \forall t$, where Δ is the period of the limit cycle.

Regular (or tonic) spiking orbits: Attracting limit cycles which have $v < 0$ for some segment of the orbit and which have $v(t^*) = v_{\rm th}$ at precisely one value of $t^* \in [t, t+\Delta]\ \forall t$, where Δ is the period of the limit cycle.

n-Spike bursting orbits: Attracting limit cycles which have $v < 0$ for some segment of the orbit and which have $v(t^*) = v_{\rm th}$ at precisely n values of $t^* \in [t, t+\Delta]\ \forall t$, where Δ is the period of the limit cycle.

Sub-threshold oscillations: Attracting limit cycles which have $v < v_{\rm th}$ along the entire orbit.

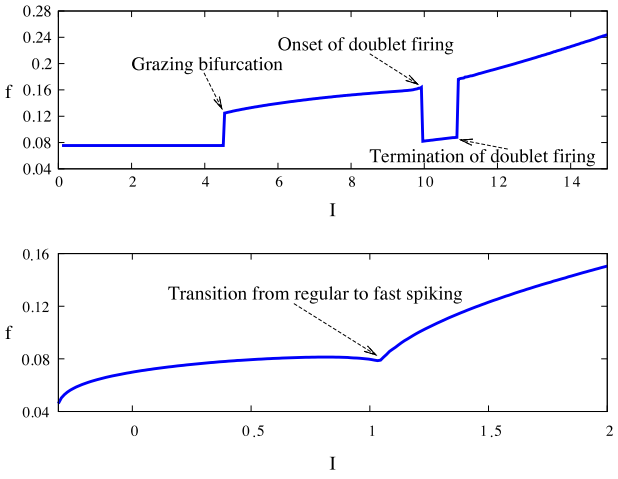

Fig. 7. Variation of the firing frequency under variation of the drive I for: Top: $\beta = 1.2$, Bottom: $\beta = 0.9$. We can clearly see how the firing rate changes as we move between solution types, and that the firing rate of the model during fast spiking is much more sensitive to changes in I than in the regular spiking mode.

The fast spiking orbits are so called as they may have arbitrarily fast frequency, whereas the frequency of regular spiking orbits must be finite. With increasing I the model can make a transition from regular to fast spiking. Contrary to the case for smooth systems, periodic orbits in discontinuous systems need not enclose a fixed point. In fact, the reset mechanism of the PWL-IF model allows for periodic orbits of (9) in the absence of any fixed points. For $\beta < 1$, the $f - I$ curve (regular spiking) reaches a maximum value before a bifurcation to fast spiking occurs. The switch between the two modes for $\beta > 1$ may have a further signature of doublet (2-spike burst) firing (which we shall consider in more detail below), and leads to a discontinuous $f-I$ curve. Fig. 7 depicts the $f - I$ curve for differing values of β under variation of I. We can clearly see the transitions between the different oscillatory regimes, particularly for $\beta = 1.2$, where we observe discontinuities in the frequency response at a grazing bifurcation, and at the onset and termination of doublet firing.

In order to characterise where in parameter space different types of solution exist, it is useful to consider the different types of bifurcation that can occur. The v-nullcline has a characteristic 'V' shape, whilst the a-nullcline is a straight line with slope β. By inspection, we see that there may exist one, two or no fixed points of (9) with f defined as in (21). There is a slight subtlety, in that the nullclines may intercept where $v > v_{\rm th}$, generating a *virtual* fixed point. From here on we refer to the branch of the v-nullcline with $v < 0$ ($v > 0$) as the left (right) v-branch. Since the system is PWL we may easily construct the eigenvalues of fixed points, where they exist, as

$$2\lambda_{\pm} = \begin{cases} 1-\omega \pm \sqrt{(1-\omega)^2 - 4\omega(\beta-1)}, & v > 0, \\ -s-\omega \pm \sqrt{(s+\omega)^2 - 4\omega(\beta+s)}, & v < 0. \end{cases} \tag{22}$$

Thus fixed points on the left v-branch are always stable, and the stability of fixed points on the right v-branch depends on the sign of $1 - \omega$. The exact nature of the fixed points is determined by the sign of the expression under the square root. Since β must be less than 1 to have two fixed points, the fixed point on the right v-branch is a saddle.

The sub-threshold dynamics are described by a continuous but non-differentiable system, so that the Jacobian matrix (around a fixed point) at the border separating linear subsystems is not defined. We shall call this border the *switching manifold*, as crossing it causes a discontinuous change in the Jacobian. Nonsmooth bifurcations can occur as fixed points or limit cycles touch the switching manifold under parameter variation. Importantly, the presence of a firing threshold in IF systems means that other nonsmooth bifurcations, and in particular grazing bifurcations as discussed in Section 3, can arise.

The PWL-IF can generate periodic behaviour via a Hopf bifurcation (HB) of a fixed point on the right v-branch when $\omega = 1$ (with $\beta > 1$) or through a discontinuous Hopf-like (dHB, black line in Fig. 8) bifurcation at $I = 0$ (with $\omega < 1$). We describe the second of these as being discontinuous since the Jacobian around the fixed point changes discontinuously. The emergent sub-threshold limit cycle crosses through the switching manifold $v = 0$. Interestingly, with a variation in I, the frequency of the limit cycle does not change (and see [8] for a proof of this), whilst the amplitude grows linearly with I. As the limit cycle grows it can tangentially touch the firing threshold, causing a grazing bifurcation, whereupon sub-threshold oscillations are replaced by regular spiking solutions. In Fig. 8 we may observe both the dHB (black) and the grazing bifurcation (blue) in (I, β) parameter space.

Bistability can arise between a stable fixed point on the left v-branch and a fast spiking orbit when $\beta > 1$ and $I < 0$. In this parameter regime, there exists a saddle node on the right v-branch, which is key in delineating the basins of attraction of the two attractors. The basin of attraction of the stable fixed point is the set of initial data such that trajectories reach threshold and are subsequently reset to the right of the separatrix of the saddle on the right v-branch. A homoclinic bifurcation (HC), indicated by the blue curve in Fig. 8, will occur when the spiking limit cycle collides with the saddle, resulting in a homoclinic orbit from the saddle at the bifurcation point. Another form of bistability is also possible in this parameter regime, namely when a regular spiking limit cycle encloses the stable fixed point. The basin of attraction of this limit cycle is the set of points such that trajectories reach threshold and are reset to the right of the separatrix of the saddle (which is also enclosed by the stable spiking orbit). Numerical studies suggest that the regular spiking orbit is lost as the basin of attraction of the stable fixed point grows and touches the orbit, and as such we shall call this an orbit crisis. As with the HC bifurcation, after this point all trajectories will tend towards the stable fixed point. A plot of the basins of attraction of the two attractors is shown in Fig. 9, whilst a plot of parameter values for which we have an orbit crisis is depicted by the magenta (OC) curve in Fig. 8. For $\beta < 1$, we have a discontinuous saddle node bifurcation (dSN, orange line in Fig. 8) at $I = 0$ where the saddle and stable fixed point come together and annihilate one another. We refer to this as a discontinuous bifurcation owing to the fact that the Jacobian of the system is undefined at the bifurcation point. For $I > 0$ there are no fixed points, and the only attractor is either the regular spiking or fast spiking orbit, dependent on the value of β. If $\beta > 1$ then the system only possesses one fixed point, which may be on the left or right v-branch dependent on the sign of I. As I crosses 0 from below, there are three scenarios: either $\omega > 1$, in which case no change of stability occurs and trajectories tend to the fixed point, else $\omega < 1$ and the fixed point becomes unstable. We either may observe sub-threshold oscillations or spiking oscillations (either bursting or tonic) depending on the other parameter values. Using results from [47] we can say more about the sub- or super-critical nature of these bifurcations, though we do not pursue this here. As β decreases through $\beta_c = (v_{\rm th} - I)/v_{\rm th}$ the fixed point no longer exists and we see spiking solutions only.

In parameter regimes where bursting orbits are stable, spikes are added when the a value after reset of the last spike of a bursting orbit crosses some value a_c, resulting in a grazing bifurcation. The graze either occurs at $v = 0$, when the fixed point of (9), with f as in (21) is to the right of $v_{\rm R}$, or at $v = v_{\rm th}$ if the fixed point is to the left of $v_{\rm R}$. After this point, trajectories will be forced up to threshold, so that the orbit gains an additional spike. For the case

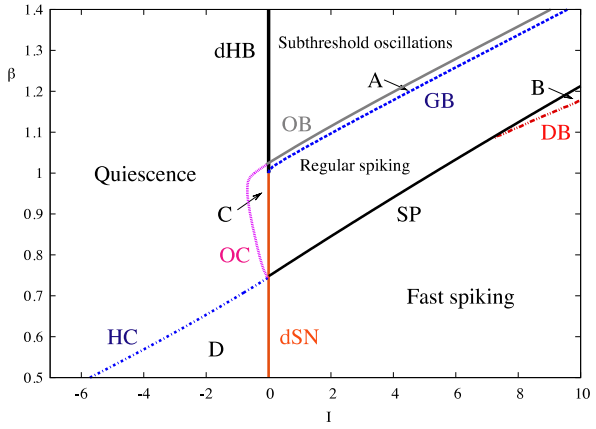

Fig. 8. Bifurcation curves showing where solution types exchange stability in the (I, β) parameter plane. Other parameters are $\omega = 0.9$, $s = 0.35$, $v_{\rm th} = 60$, $v_{\rm R} = 20$ and $k = 0.4$. The dHB refers to the discontinuous Hopf bifurcation, dSN refers to the discontinuous saddle node bifurcation, GB is the grazing bifurcation between sub-threshold oscillations and regular spiking ones, SP is the bifurcation between the regular and fast spiking solutions, HC is the homoclinic bifurcation occurring when the fast spiking orbit collides with the saddle node, OC is the orbit crisis, marking the loss of the regular spiking solution, OB is the bifurcation marking the onset/termination of bistability between sub-threshold oscillations and spiking ones, DB is the bifurcation marking the end of doublet firing, the onset of which occurs along the SP curve. Regions A, B, C, D correspond to bistable parameter regimes, the solutions of which are depicted in Fig. 10. Solution types in the other regimes are marked.

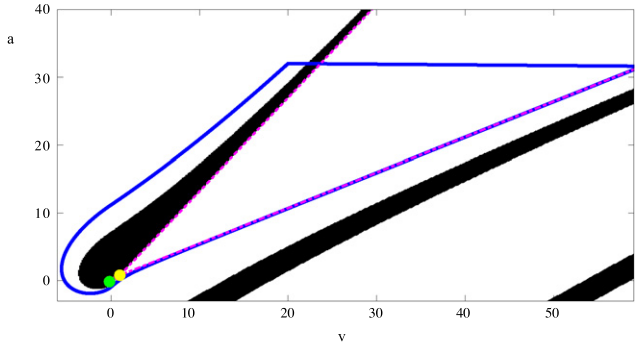

Fig. 9. Basins of attraction for the stable fixed point and limit cycle for $\omega = 0.9$, $\beta = 0.8$, $I = -0.2$, $s = 0.35$, $v_{\rm th} = 60$, $v_{\rm R} = 20$ and $k = 0.02$. Black denotes the basin of attraction of the stable fixed point whereas white denotes the basin of attraction of the limit cycle. We see that both basins are the union of disconnected sets. The green and yellow circles depict, respectively, the stable fixed point and saddle node whilst the purple dashed lines are the separatrices of the saddle node, given by the eigenvectors of the Jacobian there. The separatrix separates the basin of attraction of the two attractors. The large amplitude limit cycle is lost at the point where it touches the basin of attraction of the stable fixed point. (For interpretation of the references to colour in this figure legend, the reader is referred to the web version of this article.)

where the graze occurs at $v = 0$, the value of $a_{\rm c}$ may be found by integrating backwards from $(v, a) = (0, I)$, the point at which $(v, \dot{v}) = (0, 0)$, a time T, such that $v(-T) = v_{\rm R}$. The value of $a_{\rm c}$ is then equal to $a(-T)$. T is the flight time (in backwards time) from $v = 0$ to $v = v_{\rm R}$ and may be found numerically. For the case where the graze occurs at $v = v_{\rm th}$, the same method can be used, this time integrating from $(v, a) = (v_{\rm th}, v_{\rm th} + I)$. Interestingly, for bursting orbits, the value of $a_{\rm c}$ may also be found by finding the curves of inflection of the vector field. These curves separate trajectories that 'bend' rightwards, up to the threshold, and those which 'bend' leftwards, towards the switching manifold, and are given by the solution to the equation $\mathrm{d}^2a/\mathrm{d}v^2 = 0$. Substituting $v = v_{\rm R}$ in the resulting equation will give $a_{\rm c}$. For more discussion about inflection curves, we refer the reader to [8]. In the singular-limit as $\omega \to 0$, the inflection curve for $v > 0$ is precisely the right v-branch.

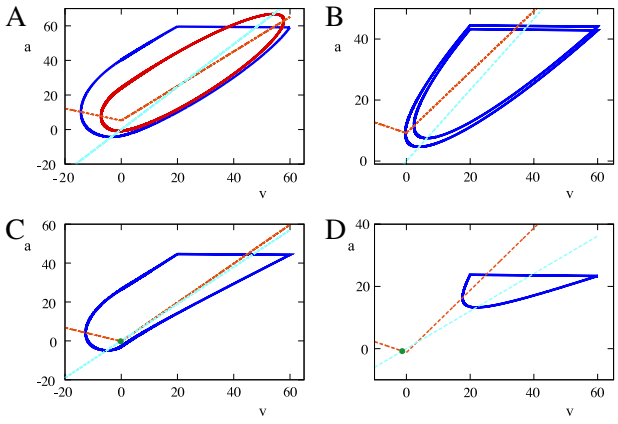

Fig. 10. Solution types in the regions indicated in Fig. 8. The blue and red solid curves indicate the periodic solutions; all solutions are stable. The orange dashed lines are the branches of the v-nullcline, whilst the sky blue dashed line depicts the a-nullcline. The green circles in the lower two figures are stable fixed points. (For interpretation of the references to colour in this figure legend, the reader is referred to the web version of this article.)

In Fig. 8, we concern ourselves only with non-bursting trajectories. In this case, the graze at $v = v_{\rm th}$ results either in the transition from sub-threshold oscillations to spiking ones, or in the transition from regular spiking orbits to a 2-spike burst. The blue (GB) curve in Fig. 8 illustrates the first of these cases in (I, β) parameter space. Where $v = 0$, a graze results in the transition from fast to regular spiking, which may occur after a window of doublet firing. The black curve (SP), in Fig. 8 corresponds to the transition to regular spiking, either from fast spiking, or from doublet firing, whereas the pink curve (DB) marks the onset/termination of doublet firing. We note that in order to have a graze at $v_{\rm th}$ we require that $\beta > \beta_c$ since we need the v-nullcline to be below the a-nullcline for $\dot{v} = 0$ in this part of the phase-plane.

The number of spikes in a burst is controlled by varying either ω, I, $v_{\rm R}$ or $v_{\rm th}$. Decreasing any of these parameters will result in bifurcations which decrease the number of spikes in a burst. Where $v_{\rm R} < 0$, the system is unable to burst as trajectories are always reset to the left of the right v-branch and are attracted to the left v-branch. We also note that we observe bursts for larger values of ω in the case where $\beta > \beta_c$ than where $\beta < \beta_c$, and that large values of I may prohibit bursting, and we observe only fast spiking, so that I and β may be used as control parameters to switch between fast spiking and burst modes.

Owing to the discontinuous nature of the flow at reset, we may observe spiking orbits that enclose all other stable attractors, be they fixed points or sub-threshold oscillations. The emergence of such orbits is controlled by the parameter k. Where k is too small, trajectories will simply tend towards the attractors whose basin of attraction they are in. However, when k is large enough, we see the emergence of large amplitude limit cycles. These occur as the flows get 'interrupted' as they head towards an attractor in the sub-threshold system. All trajectories starting outside these limit cycles are in the basin of attraction of such orbits.

We illustrate in Fig. 10 the stable solutions in the various regions of parameter space indicated in Fig. 8. The curves in Fig. 8 are generated by numerical continuation of solutions obtained from the firing map discussed later in Section 6.

5. Periodic orbits and phase response curves

To solve the PWL-IF model it is useful to recast the dynamics in matrix form so that:

$$\dot{X} = \begin{cases} A_1 X + \mu & X_1 \geq 0, \\ A_2 X + \mu & X_1 < 0, \end{cases} \tag{23}$$

where

$$A_1 = \begin{bmatrix} 1 & -1 \\ \omega\beta & -\omega \end{bmatrix}, \qquad A_2 = \begin{bmatrix} -s & -1 \\ \omega\beta & -\omega \end{bmatrix}, \quad \mu = \begin{bmatrix} I \\ 0 \end{bmatrix}, \tag{24}$$

with X_i referring to the ith component of X (i.e. $X_1 = v$ and $X_2 = a$). The solution to the equation $\dot{X} = MX + \mu$ can be written using matrix exponentials in the form

$$X(t) = G(t)X(0) + K(t)\mu, \tag{25}$$

where

$$G(t) = \mathrm{e}^{Mt}, \qquad K(t) = \int_0^t G(s)\mathrm{d}s. \tag{26}$$

Explicit solutions for G and K are easily constructed (and see for example [7]). Hereafter, we refer to G^i, K^i as the above expressions with the respective matrix $M = A_i$. To find a fast spiking orbit of period Δ (in response to constant forcing) we need only solve $(X_1(\Delta), X_2(\Delta)) = (v_{\rm th}, a_0 - k)$ subject to $(X_1(0), X_2(0)) = (v_{\rm R}, a_0)$, which gives a pair of simultaneous equations for (Δ, a_0) as:

$$v_{\rm th} = G^1_{11}(\Delta)v_{\rm R} + G^1_{12}(\Delta)a_0 + K^1_{11}(\Delta)I, \tag{27}$$

$$a_0 = \frac{G^1_{21}(\Delta)v_{\rm R} + K^1_{21}(\Delta)I + k}{1 - G^1_{22}(\Delta)}. \tag{28}$$

Bursting orbits may be constructed using similar ideas, though with more book-keeping to keep track of the sub-trajectories (each determined by a linear system) that build the full periodic orbit. For example, for an orbit with 'times-of-flight' T_i^*, $i = 1, \ldots, N$, (defined by the time spent in a region of phase space before meeting $v = 0$ or $v = v_{\rm th}$) describing a bursting orbit with $N - 2$ spikes then we have to solve for the unknowns $(T_1^*, \ldots, T_N^*, a_0)$ using a system of equations of the form

$$\begin{bmatrix} 0 \\ a_1 \end{bmatrix} = G^1(T_1^*)\begin{bmatrix} v_{\rm R} \\ a_0 \end{bmatrix} + K^1(T_1^*)\mu,$$
$$\begin{bmatrix} 0 \\ a_2 \end{bmatrix} = G^2(T_2^*)\begin{bmatrix} 0 \\ a_1 \end{bmatrix} + K^2(T_2^*)\mu,$$
$$\begin{bmatrix} v_{\rm th} \\ a_3 \end{bmatrix} = G^1(T_3^*)\begin{bmatrix} 0 \\ a_2 \end{bmatrix} + K^1(T_3^*)\mu,$$
$$\vdots$$
$$\begin{bmatrix} v_{\rm th} \\ a_n \end{bmatrix} = G^1(T_n^*)\begin{bmatrix} v_{\rm R} \\ a_{n-1} + k \end{bmatrix} + K^1(T_n^*)\mu, \tag{29}$$

for $n = 4, \ldots, N$ subject to $a_0 = a_N + k$. The period of the orbit is simply $\Delta = \sum_{i=1}^N T_i^*$.

It is common practice in neuroscience to then characterise a neuronal oscillator in terms of its phase response to a perturbation. This gives rise to the notion of a phase response curve (PRC). The PRC quantifies the phase shift of an oscillator due to a small, brief perturbation as a function of the phase of the oscillator when the perturbation occurred. A positive phase response indicates an advancement in the timing of the next oscillation, while negative values indicate a delay. For a detailed discussion of PRCs we refer the reader to [48]. One way to compute them for a given smooth dynamical system is via the Malkin adjoint method. Following [49] we briefly review this approach. Consider a smooth dynamical system $\dot{z} = F(z), z \in \mathbb{R}^n$, with a Δ-periodic solution $Z(t) = Z(t + \Delta)$ and introduce an infinitesimal perturbation Δz_0 to the trajectory $Z(t)$ at time $t = 0$. This perturbation evolves according to the linearised equation of motion:

$$\frac{\mathrm{d}\Delta z}{\mathrm{d}t} = \mathrm{D}F(Z(t))\Delta z, \qquad \Delta z(0) = \Delta z_0. \tag{30}$$

Here $\mathrm{D}F(Z)$ denotes the Jacobian of F evaluated along Z. Introducing a time-independent phase shift $\Delta\theta$ as $\theta(Z(t) + \Delta z(t)) - \theta(Z(t))$, we have to first order in Δz that

$$\Delta\theta = \langle Q(t), \Delta z(t)\rangle, \tag{31}$$

where $\langle\cdot,\cdot\rangle$ defines the standard inner product, and $Q = \nabla_Z\theta$ is the gradient of θ evaluated at $Z(t)$. Taking the time-derivative of (31) gives

$$\left\langle \frac{\mathrm{d}Q}{\mathrm{d}t}, \Delta z \right\rangle = -\left\langle Q, \frac{\mathrm{d}\Delta z}{\mathrm{d}t} \right\rangle = -\langle \mathrm{D}F^T(Z)Q, \Delta z\rangle. \tag{32}$$

Since the above equation must hold for arbitrary perturbations, we see that the gradient $Q = \nabla_Z\theta$ satisfies the linear equation

$$\frac{\mathrm{d}Q}{\mathrm{d}t} = -\mathrm{D}F^T(Z(t))Q, \tag{33}$$

subject to the conditions $Q^T(0)F(z(0)) = 1/\Delta$ and $Q(t) = Q(t + \Delta)$. The first condition simply guarantees that $\dot{\theta} = 1/T$ (at any point on the periodic orbit), and the second enforces continuity (and periodicity). The (vector) PRC, R, is related to Q according to the simple scaling $R = Q\Delta$. In general (33) must be solved numerically to obtain the PRC, say, using the *adjoint* routine in XPP [50]. However, for PWL models $\mathrm{D}F(Z)$ is piecewise constant, and we can obtain a solution in closed form [7]. Moreover it is also possible to extend the Malkin method to treat an IF process [32], which would give rise to a discontinuous PRC (at the spike time). In this latter case the continuity condition is swapped in favour of enforcing the normalisation condition $Q^T(t)F(z(t)) = 1/\Delta$ for all t.

For the PWL-IF model we may construct Q in given regions of phase space according to the prescription $Q(t) = J(T_i^* - t)Q(T_i^*)$, where $J = G^T$ (and see [7] for further details). Enforcing the normalisation condition at the times T_i^* is enough to define a periodic (yet discontinuous) form for Q. For example, for a simple tonic spiking orbit we see that solving (33) and imposing the normalisation condition at $t = 0$ and $t = \Delta$ gives a system of two linear equations in (q_1, q_2), where q_i are the components of Q as

$$q_1(\Delta)(v_{\rm th} + I - a_0 + k) + q_2(\Delta)\omega(\beta v_{\rm th} - a_0 + k) = \frac{1}{\Delta},$$
$$q_1(0)(v_{\rm r} + I - a_0) + q_2(0)\omega(\beta v_{\rm r} - a_0) = \frac{1}{\Delta}. \tag{34}$$

Using the further result that $Q(0) = \Gamma Q(T)$ where $\Gamma = J^1(\Delta)$ for fast spiking orbits or $\Gamma = J^1(T_3^*)J^2(T_2^*)J^1(T_1^*)$ for regular spiking orbits, gives

$$q_2(\Delta) = \frac{r_1 - r_2\Gamma_{11} - r_4\Gamma_{21}}{T(r_1(\Gamma_{12}r_2 + r_4\Gamma_{22}) - (r_3r_2\Gamma_{11} + r_3r_4\Gamma_{21}))},$$
$$q_1(\Delta) = \frac{1}{r_1}\left(\frac{1}{\Delta} - r_3q_2(\Delta)\right), \tag{35}$$

where

$$r_1 = v_{\rm th} + I - a_0 + k, \qquad r_2 = v_{\rm R} + I - a_0, \tag{36}$$
$$r_3 = \omega(v_{\rm th} - a_0 + k), \qquad r_4 = \omega(v_{\rm R} - a_0). \tag{37}$$

Hence for a fast spiking orbit the adjoint is given by $Q(t) = J(\Delta - t)Q(\Delta)$ and for a regular spiking orbit the corresponding Q is

$$Q(t) = \begin{cases} J^1(T_1^* - t)J^2(T_2^*)J^1(T_3^*)Q(\Delta) & 0 \le t \le t_1 \\ J^2(T_2^* - t)J^1(T_3^*)Q(\Delta) & t_1 \le t \le t_2 \\ J^1(T_3^* - t)Q(\Delta) & t_2 \le t \le \Delta \end{cases}, \tag{38}$$

where $t_j = \sum_{i=1}^j T_i^*$. In both cases the form of $Q(\Delta)$ is given by (35). PRCs for bursting solutions may be constructed in the

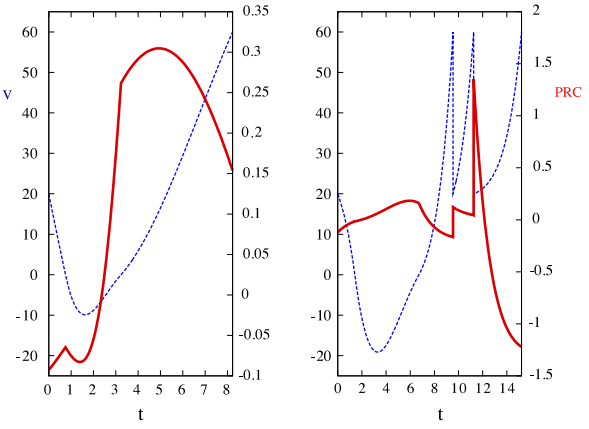

Fig. 11. Left: Voltage component of the phase response curve for a regular spiking orbit (red, solid). Right: Voltage component of the phase response curve for a 3-spike bursting orbits (red, solid). Parameter values are $\beta = 1.1, s = 0.35, k = 0.4$ and $\omega = 1$ for the regular spiking orbit and $\omega = 0.25$ for the bursting orbit. Corresponding orbits are shown in dashed blue. (For interpretation of the references to colour in this figure legend, the reader is referred to the web version of this article.)

same way, except that discontinuities are now not isolated to the ends of the periodic orbit, and so we must enforce both the normalisation condition just before and just after each threshold crossing. Typically, when studying neural oscillators, we are primarily concerned with the first (voltage) component of Q, since perturbations to the system are usually given by changes in the external current, which acts only on the voltage variable. As an example we plot in Fig. 11 the voltage component of Q for a regular spiking orbit and a burst containing three spikes. Knowledge of the PRC is fundamental in building network descriptions of weakly coupled oscillators [51], and for PWL models is discussed in more detail in [7].

To study the stability of tonic spiking orbits (and for simplicity we focus here on the case that $v > 0$), we rewrite Eq. (23) as

$$\frac{\mathrm{d}X}{\mathrm{d}t} = MX + \mu + \mathrm{d}\sum_n \delta(t - T_n), \qquad t \geq 0, \tag{39}$$

with

$$d = \begin{bmatrix} v_{\mathrm{R}} - v_{\mathrm{th}} \\ k \end{bmatrix}. \tag{40}$$

Integrating Eq. (39) between two successive firing times yields the closed form expression

$$X^-(T_{n+1}) = G(\Delta_n)[X^-(T_n) + d] + K(\Delta_n)\mu, \tag{41}$$

with $\Delta_n = T_{n+1} - T_n$. The superscript on X in Eq. (41) indicates that we evaluate X at the firing event *before* the reset, i.e. $X^-(T_n) = \lim_{\varepsilon \searrow 0} X(T_n - \varepsilon)$. For later reference, we here also introduce $X^+(T_n) = \lim_{\varepsilon \searrow 0} X(T_n + \varepsilon)$ and note that $X^+(T_n) = d + X^-(T_n)$. A perturbation of the periodic orbit s with a period Δ leads to perturbed firing times $\widetilde{T}_n$, for which we make the ansatz $\widetilde{T}_n = n\Delta + \delta T_n$. Similarly, we write the perturbed trajectory as $\widetilde{X}(t) = s(t) + \delta X$. Hence, we have from Eq. (41)

$$\widetilde{X}^-(T_{n+1}) = G(\widetilde{\Delta}_n)[\widetilde{X}^-(\widetilde{T}_n) + d] + K(\widetilde{\Delta}_n)\mu, \tag{42}$$

where $\widetilde{\Delta}_n = \widetilde{T}_{n+1} - \widetilde{T}_n$. Linearising equation (42) then results in

$$\delta X_{n+1} = \mathrm{e}^{M\Delta}\delta X_n - \delta T_n \mathrm{e}^{M\Delta} p + \delta T_{n+1} q, \tag{43}$$

with

$$p = M[s^-(\Delta) + d] + \mu = \dot{s}^+(\Delta), \tag{44a}$$

$$q = Ms^-(\Delta) + \mu = \dot{s}^-(\Delta), \tag{44b}$$

where δX_n is defined through $\widetilde{X}(T_n) = s(T_n) + \delta X_n$ and $\dot{s} = \mathrm{d}s/\mathrm{d}t$. At first sight, Eq. (43) appears to be implicit since δX_{n+1} is given in terms of the unknown perturbation of the firing time δT_{n+1}. However, we need to solve Eq. (43) with the constraint that $\widetilde{v}(\widetilde{T}_n^-) = v_{\mathrm{th}} = v(T_n^-)$, so that the first component of δX_{n+1} vanishes. Defining the row vector γ with components $\gamma_i = -[\mathrm{e}^{M\Delta}]_{1i}/[q]_1$, we find for the perturbed firing time

$$\delta T_{n+1} = \gamma(\delta X_n - p\delta T_n), \tag{45}$$

which immediately leads to

$$\delta X_{n+1} = (\mathrm{e}^{M\Delta} + q\gamma)(\delta X_n - p\delta T_n). \tag{46}$$

Hence, the perturbations of X at the $(n+1)$th firing time are uniquely determined by the perturbations at the nth firing event. From Eq. (45), we see that

$$\delta X_n - p\delta T_n = (\mathrm{e}^{M\Delta} - M\mathrm{d}\gamma)(\delta X_{n-1} - p\delta T_{n-1}). \tag{47}$$

Without loss of generality, we set $\delta T_0 = 0$ at $t = 0$, which is equivalent to saying that there is some perturbation of the periodic orbit at $t = 0$. Then, Eqs. (45) and (46) yield $\delta T_1 = \gamma\delta X_0$ and $\delta X_1 = (\mathrm{e}^{M\Delta} + q\gamma)\delta X_0$, so that we find from Eqs. (46) and (47)

$$\delta X_{n+1} = (\mathrm{e}^{M\Delta} + q\gamma)(\mathrm{e}^{M\Delta} - M\mathrm{d}\gamma)^n \delta X_0. \tag{48}$$

Hence, the perturbations grow without bound if there is at least one eigenvalue of $B = (\mathrm{e}^{M\Delta} - M\mathrm{d}\gamma)$ with modulus larger than one. Conversely, if all eigenvalues of B have moduli smaller than one, then any initial perturbation decays towards zero. However, our analysis indicates that B always possesses exactly one eigenvalue equal to 1, so that B^n converges against a constant matrix $\bar{B}$ for large n instead of decaying if all other eigenvalues have moduli smaller than one. The stability of the period one orbit is then determined by the product $(\mathrm{e}^{M\Delta} + q\gamma)\bar{B}$. For the parameter values where fast spiking orbits exist (e.g. $I = 4.0, k = 0.4, v_{\mathrm{th}} = 60, v_{\mathrm{R}} = 8.1, \beta = 0.5, s = 0.35, \omega = 0.08$) we find that this product equals zero, so that the orbit is asymptotically stable. The above argument relies on the numerical evaluation of the matrices and eigenvalues. A more detailed study on the structure of B will be reported elsewhere.

Next we show how to determine single neuron behaviour (existence and stability) via an alternative approach based on the construction of a discontinuous one-dimensional return map.

6. Firing map

Due to the nature of the nonsmooth dynamics of the system at reset, it is useful to consider a map of the adaptation variable at successive firing times. This will collapse the dynamics of the full system to a one-dimensional return map. This has previously been considered by Touboul and Brette [52] for a broad class of planar nonlinear IF models. Here, we focus on the construction of such a map for the PWL-IF model. We consider a set, called the Poincaré section, $\Sigma = \{(v, a) | v = \bar{v} \in \mathbb{R}\}$ which is transverse to the flow for all $(\bar{v}, a) \in \Sigma$. The value of $\bar{v}$ above is arbitrary, so that our section may be placed anywhere in the phase plane. The first return map is a function which gives, for each value $a_0 \in \mathbb{R}$, the value of a at the next intersection with Σ, of a trajectory starting from $(\bar{v}, a_0)$. The second return map gives the second intersection of such a trajectory with Σ and so forth. We refer to the firing map as the first return map with $\bar{v} = v_{\mathrm{R}}$. We note that trajectories will not intersect v_{R} upon reaching threshold, but are reset discontinuously to it, and thus we may consider intersection of the trajectory with $\Sigma_1 = \{(v, a) | v = v_{\mathrm{th}}\}$ and apply the reset conditions to give the value of a we seek. Suppose that the trajectory starting from (v_{R}, a_n) reaches threshold at time Δ_n. Defining the firing map as

the unique function $P : \mathbb{R} \to \mathbb{R}$ such that $P(a_n) = a(\Delta_n) + k$, we have

$$P(a) = \begin{cases} G^1_{21}(\Delta_n)v_R + G^1_{22}(\Delta_n)a + K^1_{21}(\Delta_n)I + k & a < a_c, \\ G^1_{22}(T^*_3)a^* + K^1_{21}(T^*_3)I + k & a > a_c, \end{cases} \quad (49)$$

where T^*_3 is the flight time from $v = 0$ to $v = v_{th}$ and

$$a^* = G^2_{22}(T^*_2)(G^1_{21}(T^*_1)v_R + G^2_{22}(T^*_1)a + K^1_{21}(T^*_1)I) + K^2_{21}(T^*_2)I, \quad (50)$$

where T^*_1 is the flight time from $v = v_R$ to $v = 0$ and T^*_2 is the total flight time in the region $v < 0$. The flight times are given by the solutions to transcendental equations are not available in an explicit form, and so we find the values of T^*_1, T^*_2 and T^*_3 numerically.

The point a_c above is the same as the one described in Section 4, and separates trajectories, starting from (v_R, a), which cross the switching manifold from those which do not. At $a = a_c$, the map may have a discontinuity, dependent on the pair (β, ω). For the map to be discontinuous, we require that the fixed point lies to the left of v_R, and that the matrix A_1 has real eigenvalues. An example of such a map is depicted in Fig. 12.

Fixed points of the map are found by solving $\bar{a} = P(\bar{a})$, and the points are stable if $|J(\bar{a})| < 1$ where $J(\bar{a}) = P'(\bar{a})$. Fixed points of the map may lose stability via a tangent bifurcation where $J(\bar{a}) = 1$ or a period-doubling bifurcation where $J(\bar{a}) = -1$. They can also be lost as they pass through the discontinuity at $a = a_c$.

In order to characterise the stability of the fixed points, we first need to find an expression for $J(a)$. We have, upon setting $a_n = a$, $\Delta_n = \Delta$, for $a < a_c$ that:

$$\begin{bmatrix} v_R \\ P(a) \end{bmatrix} = G^1(\Delta)\begin{bmatrix} v_R \\ a \end{bmatrix} + K^1(\Delta)\mu + \begin{bmatrix} v_R - v_{th} \\ k \end{bmatrix}. \quad (51)$$

Differentiating this equation with respect to a yields:

$$\begin{bmatrix} 0 \\ J(a) \end{bmatrix} = G^1(\Delta)\begin{bmatrix} 0 \\ 1 \end{bmatrix} + \frac{d\Delta}{da}\left\{A_1 G^1(\Delta)\begin{bmatrix} v_R \\ a \end{bmatrix} + G^1(\Delta)\mu\right\}. \quad (52)$$

We may solve the first of the above equations to find an expression for $d\Delta/da$ after which we may then use the second equation to define $J(a)$ in terms of $d\Delta/da$. A similar process determines $J(a)$ for $a > a_c$ (taking care to piece together solutions and derivatives across $v = 0$). We observe a qualitatively similar form of the firing map to that found by Medvedev [53] for the Chay–Keizer model [54,55] (for bursting in a pancreatic β-cell). The map may be thought of as divided into two portions at a_c, with the left hand portion, with $a < a_c$, attaining some maximum value and the right hand portion having a small and negative slope. Fixed points may exist in either portion, and it is easy to construct scenarios in which fixed points 'disappear' across the discontinuity. As an example, we plot in Fig. 12 the first, second, third and fourth return maps in a parameter regime that supports a stable burst with 3 spikes. We see three fixed points on the third return map, corresponding to the a-values at the spike times.

Stable fixed points on the left hand portion of the map correspond to fast spiking solutions, whilst those on the right correspond to regular spiking solutions. We note that under parameter variation, it is possible to generate unstable fixed points in the right hand portion of the map. In this parameter regime, we observe doublet firing, the onset of which is marked by a period-doubling bifurcation. Shown in Fig. 13 is the representation of doublets in the return maps. We plot both the first and second return maps, along with their respective first derivatives. There exists an unstable fixed point in the first return map, and two stable fixed points in the second, corresponding to the doublet. As I is increased (decreased), the fixed point in the first return map will move leftward (rightward) and stabilise so that the fast (regular) spiking solution becomes stable and we lose the doublet.

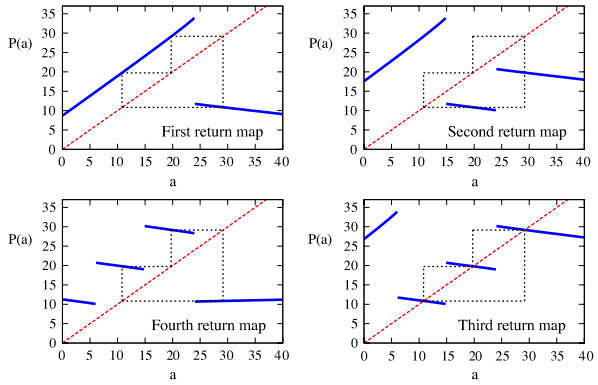

Fig. 12. First, second, third and fourth return maps at $\omega = 0.19$, $\beta = 1.2$, $I = 4$, $s = 0.35$ and $k = 0.4$. We see three stable fixed points on the third return map, (dashed cobwebs) corresponding to a 3-spike burst.

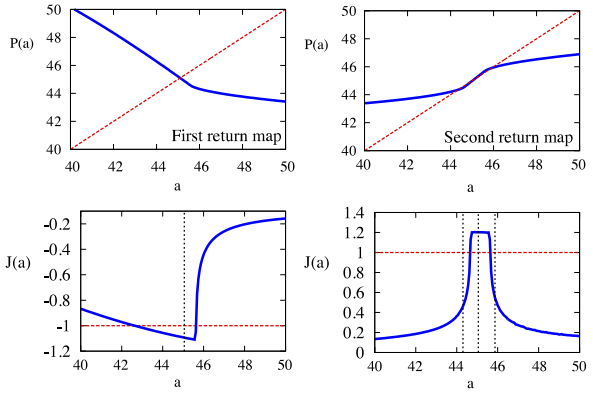

Fig. 13. First and second return maps (top), together with their first derivatives (bottom), for the doublet firing parameter regime with $\omega = 0.9$, $\beta = 1.2$, $I = 10$, $k = 0.04$ and $s = 0.35$. The vertical dashed lines in the lower figures indicate where the fixed points of the maps are. We can see the fixed point in the first return map is unstable. Of the three fixed points in the second return map, we observe that one unstable fixed point, corresponds to the unstable fixed point in the first return map, along with a pair of stable fixed points, corresponding to a doublet.

The bifurcation to doublet firing occurs as fast spiking orbits approach the switching manifold. We may track the onset and termination of doublet firing in (I, β) parameter space by continuing the steady states for which $J(\bar{a}) = -1$. We find that for a given value of β there are necessarily two bifurcation branches; one to mark the onset and one to mark the termination of doublet firing. We also observe that below some value of β, the model no longer fires in doublets, and the transition from regular to fast spiking occurs exactly as the fast spiking orbit grazes the switching manifold. Here, all of the steady states have $J(\bar{a}) > -1$. The bifurcation in the firing map is a little subtler here. We see that the map is no longer discontinuous. The bifurcation from regular to fast spiking in this case is marked by a discontinuous change in $J'(\bar{a})$ as the fixed point moves from the right to the left portion of the map.

As well as doublet firing, we often have bistability of periodic attractors near bifurcations, as can be seen in the top panel of Fig. 10, in which the sub-threshold oscillation and spiking orbit are both stable. Since we cannot always 'see' sub-threshold attractors with the firing map, we may repeat the same methodology, setting $\bar{v} = 0$, thus moving the Poincaré section to $\Sigma_2 = \{(v, a)|v = 0\}$. The emergence of the spiking orbit is marked, as for doublet firing, by the passing of a steady state through $J(\bar{a}) = -1$ so we may track this point in parameter space to give us the boundary on which this occurs. The grazing bifurcation, resulting in the loss of the stable sub-threshold oscillation occurs as the fixed point corresponding to the sub-threshold oscillation crosses the discontinuity in the

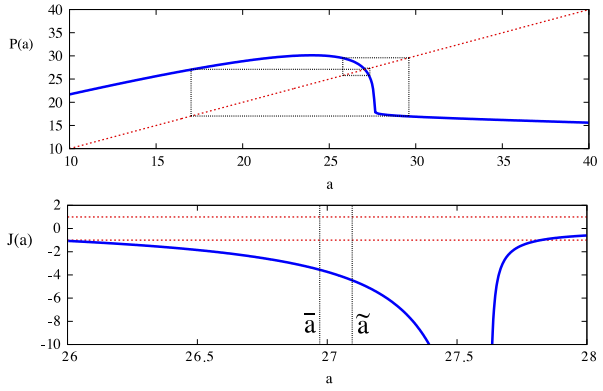

Fig. 14. A snap-back repeller. Top: Firing map, Bottom: First derivative of the firing map. We see the presence of an unstable fixed point $\bar{a}$, in conjunction with a point $\tilde{a}$ in its repelling neighbourhood such that $P^4(\tilde{a}) = \bar{a}$. It may be shown that the first derivative of the evolution of $\tilde{a}$ under P is nowhere equal to zero. Parameter values here are $I = 4$, $\beta = 0.9$, $\omega = 0.4$, $s = 0.35$ and $k = 0.4$. The vertical dashed lines on the bottom plot indicate the location of $\bar{a}$ and $\tilde{a}$. The chaotic orbit with these parameters is shown in Fig. 15.

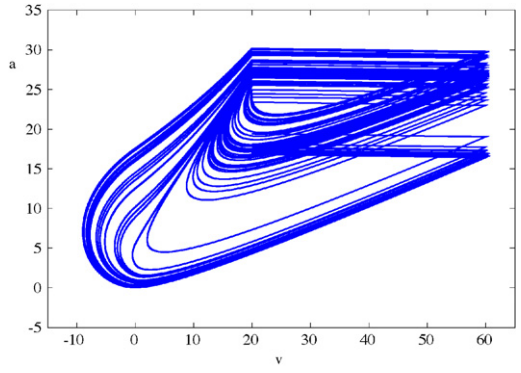

Fig. 15. The chaotic orbit associated with the snap-back repeller in Fig. 14.

return map. Thus, unlike the spiking solution, the sub-threshold oscillation is always stable where it exists. This does not, however, preclude the existence of unstable sub-threshold limit cycles, which we may expect when the dHB is subcritical. We may then observe where the fixed point 'disappears' to track where in parameter space the grazing bifurcation occurs. Interestingly, we note that the system may already be in a bistable regime as the dHB occurs.

The firing map is of the type that allows for a snap-back repeller, and as such will support chaotic solutions [56]. To define such a snap-back repeller suppose $\bar{a}$ is a fixed point of P with $|P'(\bar{a})| > 1$, and suppose there exists a point $a \neq \bar{a}$ in a repelling neighbourhood of $\bar{a}$, such that $a_M = \bar{a}$ and $P'(a_k) \neq 0$ for $1 \leq k \leq M$, where $a_k = P^k(a_0)$. Then $\bar{a}$ is called a snap-back repeller of P. Zheng and Tonnelier [57] have shown the presence of snap-back repellers in the QIF model with adaptation. Given the similarities between the PWL-IF model and the QIF with adaptation, we may expect similar properties. We show an example of such a point in the PWL-IF model in Fig. 14, along with an associated chaotic orbit in Fig. 15. We shall now use the notion of Lyapunov exponents in nonsmooth systems to demonstrate where chaotic solutions exist in the PWL-IF model.

7. Maximal Lyapunov exponents

The presence of chaos in a dynamical system may be characterised in terms of Lyapunov exponents (LEs). LEs measure the exponential rates of divergence of nearby orbits of an attractor in state space. Stable equilibria have only negative LEs, periodic attractors have one zero exponent, whilst the rest are negative. Chaotic attractors, however, have at least one positive LE. Conversely, where the attractor has at least one positive LE, we expect chaotic behaviour.

LEs for continuously differentiable dynamical systems are generally calculated using the Jacobian of the system along the orbit that the flow produces, by solving a variational equation. The PWL-IF system is everywhere linear, except at $v = 0$, so that the Jacobian is piecewise constant. Owing to the discontinuity in the PWL-IF model, we must be careful when considering what happens to δX at reset, recalling that δX is a small perturbation to some orbit, which we here denote by X. In [58] a framework for studying the evolution of δX in impacting systems, in a model for which $\dot{X} = F(X)$ between impacts, was developed. This approach was applied to one-dimensional IF models in [35]. We now use this framework to develop the notion of LEs for the PWL-IF model.

In a sub-threshold regime the linearised equations of motion around a trajectory $X(t)$ satisfy

$$\frac{\mathrm{d}\delta X}{\mathrm{d}t} = \mathrm{D}F(X(t))\delta X. \tag{53}$$

Since our system is piecewise linear $\mathrm{D}F(X(t)) = M$ so that

$$\mathrm{D}F(X(t)) = \begin{cases} A_1 & v \geq 0 \\ A_2 & v < 0 \end{cases}. \tag{54}$$

We define an indicator function h as

$$h(X) = X_1 - v_{\mathrm{th}} \tag{55}$$

so that the discontinuity in the system occurs at time T where $h(X(T)) = 0$. We also define a vector function

$$g(X) = \begin{bmatrix} v_{\mathrm{R}} \\ X_2 + k \end{bmatrix}, \tag{56}$$

which governs the transition condition across the discontinuity so that $X^+(T) = g(X^-(T))$. Suppose that we have two trajectories: an unperturbed trajectory $X(t)$ and a perturbed trajectory $\widetilde{X}(t)$ such that $\delta X(t) = \widetilde{X}(t) - X(t)$, and that the unperturbed trajectory crosses threshold at time T, and the perturbed trajectory crosses at $\widetilde{T} = T + \delta t$. Writing $\delta X^- = \delta X^-(t)$ and $X^- = X^-(t)$, we have, from [58], that

$$\mathcal{H}(X^-)[\delta X^- + (A_1 X^- + \mu)\delta t] = 0, \tag{57}$$

where

$$\mathcal{H}(X^-) = \left.\frac{\partial h(X)}{\partial X^T}\right|_{X=X^-(T)}, \tag{58}$$

is the Jacobian of the indicator function. For our choice of h, this is simply the row vector $\mathcal{H}(X^-) = [1, 0]$. We then solve (59) to give:

$$\delta t = -\frac{\mathcal{H}(X^-)\delta X^-}{\mathcal{H}(X^-)(A_1 X^- + \mu)} = -\frac{\delta v^-}{v_{\mathrm{th}} + I - a^-(T)}, \tag{59}$$

where $\delta X^- = (\delta v^-, \delta a^-)$ and $X^- = (v^-, a^-)$. We note here the equivalence, upon setting $\delta T_n = 0$, of (59) and (45). Defining the Jacobian of the transition condition as

$$\mathcal{J}(X^-) = \left.\frac{\partial g(X)}{\partial X^T}\right|_{X=X^-(T)}, \tag{60}$$

we arrive at

$$\delta X^+ = \mathcal{J}(X^-)\delta X^- + [\mathcal{J}(X^-)(A_1 X^- + \mu) - (A_1 X^+ + \mu)]\delta t, \tag{61}$$

where $\delta X^+ = \delta X^+(T + \delta t)$. For $v_{\mathrm{R}} < 0$, we would replace (61) by

$$\delta X^+ = \mathcal{J}(X^-)\delta X^- + [\mathcal{J}(X^-)(A_1 X^- + \mu) - (A_2 X^+ + \mu)]\delta t. \tag{62}$$

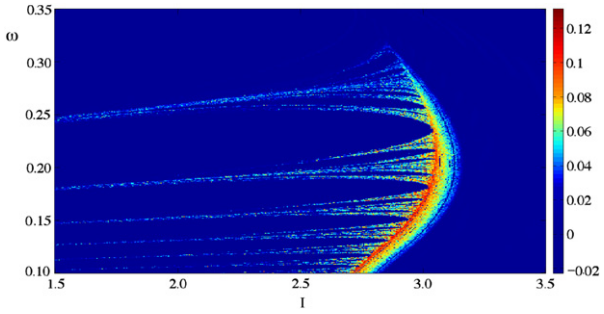

Fig. 16. Maximal Lyapunov exponent for the PWL-IF system evaluated at $\beta = 0.8, k = 0.4, v_{\rm th} = 60, v_{\rm R} = 20$ and $s = 0.35$. Light colors indicate positive values, whereas dark colors correspond to zero or negative values. We see a marked boundary of chaotic solutions. This boundary marks the transition between burst firing and fast spiking as we increase I to its critical value. We also observe chaos in transitions between different burst states.

For the PWL-IF model the matrix $\mathcal{J}$ is simply

$$\mathcal{J}(X^-) = \begin{bmatrix} 0 & 0 \\ 0 & 1 \end{bmatrix}, \tag{63}$$

so that (61), using (59) becomes

$$\delta X^+ = \begin{bmatrix} 0 \\ \delta a^- \end{bmatrix} + \frac{\delta v^-}{v_{\rm th} + I - a^-} \begin{bmatrix} v_{\rm R} + I - a^- - k \\ \omega(\beta(v_{\rm R} - v_{\rm th}) - k) \end{bmatrix}. \tag{64}$$

This is linear in δv^- and δa^-, so we may write this in matrix form as

$$\delta X^+ = K(a^-(T))\delta X^-, \tag{65}$$

where

$$K(a) = \begin{bmatrix} k_1(a) & 0 \\ k_2(a) & 1 \end{bmatrix}, \tag{66}$$

with

$$k_1(a) = \frac{v_{\rm R} + I - a - k}{v_{\rm th} + I - a}, \tag{67}$$

$$k_2(a) = \frac{\omega(\beta(v_{\rm R} - v_{\rm th}) - k)}{v_{\rm th} + I - a}. \tag{68}$$

Thus, overall the separation vector δX evolves as $G(t-T_k)K(a^-(T_k)) \cdots K(a^-(T_1))G(T_1)\delta X(0)$ for $k = 1, 2, 3, \ldots$, with $G(t) = \exp(Mt)$. The maximal LE (MLE) is then given by the natural logarithm of the modulus of the largest eigenvalue of the matrix

$$L = \lim_{k\to\infty} \frac{1}{\Delta_k} K(a^-(T_k))G(T_k) \cdots K(a^-(T_1))G(T_1), \tag{69}$$

where $\Delta_k = \sum_{i=1}^k T_i$. A plot of the MLE in the (I, ω) plane is shown in Fig. 16. In this region of parameter space, we see bursting orbits for smaller values of I whereas larger values of I prohibit bursting, so that we have 'burst death' under variation of I. We observe the presence of chaotic solutions both at this boundary where burst solutions cease to exist, marked by the large sweeping vertical arc and at the boundaries of transitions between solutions with differing numbers of spikes, marked by the thin horizontal arcs. In these regions of parameter space, we see that the firing map possesses snap-back repellers, so that the map also predicts chaos.

For a one dimensional nonlinear IF model the above analysis becomes somewhat simpler. Assume that, below threshold, a perturbed and unperturbed trajectory, $\widetilde{v}$ and v respectively, are related by the equation

$$\delta v(t) = \Phi(t, T_m)\delta v(T_m), \tag{70}$$

where $\delta v = v - \widetilde{v}$. Following the propagation of a perturbation through threshold gives (cf. Eq. (65))

$$\delta v^+ = \frac{\dot v(T_m^+)}{\dot v(T_m^-)}\delta v^-. \tag{71}$$

Hence the LE is

$$\begin{aligned} \Lambda &= \lim_{t\to\infty} \frac{1}{t} \ln \left| \frac{\delta v(t)}{\delta v(0)} \right| \\ &= \lim_{k\to\infty} \frac{1}{T_k - T_1} \sum_{m=1}^k \ln \left| \Phi(T_{m+1}, T_m) \frac{\dot v(T_m^+)}{\dot v(T_m^-)} \right|. \end{aligned} \tag{72}$$

It is informative to calculate the LE for the example of a Δ-periodic orbit in a nonlinear IF model under constant input where $\dot v = f(v) + I$. In this case, below the threshold, a perturbed and unperturbed trajectory are related by the equation

$$\int_{v(0)}^{v(t)} \frac{{\rm d}v}{f(v) + I} = \int_{\widetilde v(0)}^{\widetilde v(t)} \frac{{\rm d}v}{f(v) + I}. \tag{73}$$

For small deviations between the two trajectories we may expand (73) to obtain the result $\Phi(t, s) = \Phi(t - s)$, where

$$\Phi(t) = \frac{f(v(t)) + I}{f(v(0)) + I}. \tag{74}$$

Hence the LE is

$$\Lambda = \frac{1}{\Delta} \ln \left[\frac{f(v(\Delta)) + I}{f(v(0)) + I} \frac{\dot v(\Delta^+)}{\dot v(\Delta^-)} \right] = 0, \tag{75}$$

as expected for a periodic orbit. This result nicely illustrates that although a nonlinear IF model may have a positive exponent in the absence of a firing threshold (as would be the case for the QIF model), the firing and reset mechanism can inhibit the exponential divergence of nearby trajectories.

8. Linearly coupled networks

In this section we explore network dynamics for coupled PWL-IF neurons, with a focus on electrical synapses. An electrical synapse is an electrically conductive link between two adjacent nerve cells that is formed at a fine gap between the pre- and post-synaptic cells known as a gap junction and permits a direct electrical connection between them. They are known to be abundant in the retina and cerebral cortex of vertebrates and have been directly demonstrated between inhibitory neurons in the neocortex [59]. In fact it would appear that they are now ubiquitous throughout the human brain [60], and may play an essential role in higher brain function as originally suggested by Schmitt et al. [61]. Indeed they are currently thought to contribute to both normal [62] and abnormal physiological brain rhythms, including epilepsy [63].

Indexing neurons in a network with the label $\alpha = 1, \ldots, N$ and defining a gap junction conductance strength between neurons α and β as $g_{\alpha\beta}$ means that neuron α experiences a drive of the form $N^{-1}\sum_{\beta=1}^N g_{\alpha\beta}(v^\beta - v^\alpha)$ to the equation for $\dot v_\alpha$. For a phase locked state then $(v^\alpha(t), a^\alpha(t)) = (v(t - \phi_\alpha\Delta), a(t - \phi_\alpha\Delta))$, $(v(t), a(t)) = (v(t + \Delta), a(t + \Delta))$, (for some constant phases $\phi_\alpha \in [0, 1)$) and we have N equations distinguished by the driving terms $N^{-1}\sum_{\beta=1}^N g_{\alpha\beta}(v(t + (\phi_\alpha - \phi_\beta)\Delta) - v(t))$. For globally coupled networks with $g_{\alpha\beta} = g$ maximally symmetric solutions describing synchronous, asynchronous, and cluster states are expected to be generic [64].

8.1. Synchronous states

For global coupling, gap-junction currents vanish if all the neurons behave synchronously ($\phi_\alpha = 0$ for all α). Hence, the

period of a rhythmic network state is inherited directly from the period of a single uncoupled oscillating neuron. We may probe the stability of a synchronous network state s_N where the voltage of all N neurons is positive in a similar manner as presented in Section 5. In the synchronous network state, all neurons follow the same trajectory $s(t)$, so that s_N consists of N copies of s. Let T_n^α denote the nth firing time of the neuron with label α, $\alpha = 1, \ldots, N$, then the dynamics of the network state $Y = (v^1, a^1, \ldots, v^N, a^N)$ between T_n^α and the firing of another neuron, T_m^β, $\beta \neq \alpha$, is governed by

$$\frac{\mathrm{d}Y}{\mathrm{d}t} = \mathcal{M}Y + F + e^\alpha \otimes \mathrm{d}\delta(t - T_n^\alpha), \tag{76}$$

where $\otimes$ implies the usual tensor product and $\mathcal{M} = 1_N \otimes M + gG \otimes H$. 1_N corresponds to the identity matrix in $\mathbb{R}^{N\times N}$, and M is defined as in Eq. (39). $G \in \mathbb{R}^{N\times N}$ encodes the topology of the network, while $H \in \mathbb{N}^{2\times 2}$ determines the variables through which the coupling of strength g occurs. For example, in the case of a globally connected network all entries of G are equal to one except those on the diagonal, which are given by $(1-N)$. Since in the present model only the voltage equations are coupled and the voltage variable is the first in each state vector of a single neuron, we have

$$H = \begin{pmatrix} 1 & 0 \\ 0 & 0 \end{pmatrix}. \tag{77}$$

The $2N$ dimensional vector F consists of N copies of μ, and the only non-zero element in $e^\alpha \in \mathbb{R}^{2N}$ is at the $(2\alpha - 1)$th position. μ and d are defined as earlier (see Section 5). Integration of Eq. (76) results in

$$Y^-(T_m^\beta) = \mathrm{e}^{\mathcal{M}(T_n^\beta - T_n^\alpha)}[Y^-(T_n^\alpha) + e^\alpha \otimes d] + J, \tag{78}$$

where the integral

$$J = \int_{T_n^\alpha}^{T_m^\beta} \mathrm{e}^{\mathcal{M}(T_m^\beta - s)} F \mathrm{d}s, \tag{79}$$

can be computed by diagonalising $\mathcal{M}$. As in Section 5, we introduce perturbations of the network around the synchronous network state and of the firing times as $\widetilde{Y}(t) = s_N(t) + \delta Y$ and $\widetilde{T}_n^\alpha = nT + \delta T_n^\alpha$, respectively. When we evaluate Eq. (78) at perturbed firing times and linearise the resulting expression, we need to be careful about the order in which the neurons fire. To illustrate this point, we consider two coupled neurons and assume that none of the neurons fires twice without the other neuron reaching threshold in between. Suppose that the first neuron has just induced a spike at $\widetilde{T}_n^1$ and the second neuron is close to threshold without having fired yet. Then the second neuron crosses threshold at $\widetilde{T}_n^2$ with the *same* index n, since we perturb around the synchronous network state where all neurons fire simultaneously at $T_n = n\Delta$. When we insert these perturbed firing times into Eq. (78) and linearise it, we find

$$\delta Y_n^2 = \delta Y_n^1 + p_1(\delta T_n^2 - \delta T_n^1) + e^1 \otimes d, \tag{80}$$

with

$$p_1 = Ks_N^-(\Delta) + F + \mathcal{M}\mathrm{e}^1 \otimes d, \tag{81}$$

where δY_n^i corresponds to the perturbation of the network when the ith neuron fires for the nth time. Since Eq. (80) describes the perturbation of the network state when the second neuron reaches threshold, i.e. $\widetilde{v}^2 = v_{\mathrm{th}}$, the third component of δY_n^2 equals zero, so that

$$\delta T_n^2 = \gamma_1 \delta Y_n^1 + \delta T_n^1, \tag{82}$$

which in turn leads to

$$\delta Y_n^2 = (1_N + p_1\gamma_1)\delta Y_n^1, \tag{83}$$

where γ_1 denotes a row vector with components $[\gamma_1]_i = -[\mathrm{e}^{\mathcal{M}\Delta}]_{3i}/[p_1]_3$. The first neuron just passed through the discontinuity, so that the value of $\widetilde{X}^1(\widetilde{T}_n^2)$ is much closer to $s^+(T_n)$ than to $s^-(T_n)$. Therefore, the first two components in δY_n^2 are of the order of the discontinuity d and hence can be large. To comply with the prerequisite of small perturbations for the validity of the linear stability analysis, we introduce

$$\delta \overline{Y}_n^2 = \delta Y_n^2 - e^1 \otimes d, \tag{84}$$

the components of which are now all small. Once the second neuron has reached threshold at $\widetilde{T}_n^2$, the next time the first neuron will fire is at $\widetilde{T}_{n+1}^1$. We see from Eq. (78) that the perturbed trajectory then depends on the term

$$\widetilde{Y}^-(\widetilde{T}_n^2) + e^2 \otimes d = s_N^-(T_n) + \delta Y_n^2 + e^2 \otimes d \tag{85}$$

which we rewrite with the help of Eq. (84) as

$$\widetilde{Y}^-(\widetilde{T}_n^2) + e^2 \otimes d = s_N^+(T_n) + \delta \overline{Y}_n^2. \tag{86}$$

Here, we employ that

$$s_N^-(T_n) + e^1 \otimes d + e^2 \otimes d = s_N^+(T_n). \tag{87}$$

Inserting the perturbed firing times $\widetilde{T}_{n+1}^1$ and $\widetilde{T}_n^2$ as well as Eq. (86) into Eq. (78) and linearising the resulting expression leads to

$$\delta Y_{n+1}^1 = \mathrm{e}^{\mathcal{M}\Delta}(\delta \overline{Y}_n^2 - p_2 \delta T_n^2) + q_2 \delta T_{n+1}^1, \tag{88}$$

with

$$p_2 = Ks_N^+(\Delta) + F, \qquad q_2 = Ks_N^-(\Delta) + F. \tag{89}$$

From Eq. (80) we see that

$$\delta \overline{Y}_n^2 = \delta Y_n^1 + p_1(\delta T_n^2 - \delta T_n^1), \tag{90}$$

so that Eqs. (88) and (90) fully determine the propagation of perturbations through the network. For notational convenience, we drop the overline in Eq. (90) in the remainder of the manuscript. Since the first neuron elicits a spike at $\widetilde{T}_{n+1}^1$, the voltage variable $\widetilde{v}^1$ reaches threshold at this time. Hence, the first component of δY_{n+1}^1 vanishes, so that

$$\delta T_{n+1}^1 = \gamma_2[\delta Y_n^2 - p_2 \delta T_n^2], \tag{91}$$

where we introduce the row vector γ_2 with components $[\gamma_2]_i = -[\mathrm{e}^{\mathcal{M}\Delta}]_{1i}/[q_2]_1$. We then find from Eq. (88)

$$\delta Y_{n+1}^1 = (\mathrm{e}^{\mathcal{M}\Delta} + q_2\gamma_2)(\delta Y_n^2 - p_2 \delta T_n^2). \tag{92}$$

Moreover, the above analysis leads to the recursion relation

$$(\delta Y_n^2 - p_2 \delta T_n^2) = B_N(\delta Y_{n-1}^2 - p_2 \delta T_{n-1}^2), \tag{93}$$

with

$$B_N = (1_N + p_1\gamma_1 - p_2\gamma_1)(\mathrm{e}^{\mathcal{M}\Delta} + q_2\gamma_2) - p_2\gamma_2, \tag{94}$$

which immediately results in

$$\delta Y_{n+1}^1 = (\mathrm{e}^{\mathcal{M}\Delta} + q_2\gamma_2)B_N^n \delta Y_0. \tag{95}$$

In arriving at Eq. (95) we assumed without loss of generality that there is some perturbation δY_0 at $t = 0$ such that the first neuron fires first, i.e. $\widetilde{T}_1^1 < \widetilde{T}_1^2$, so that $\delta T_1^1 = \gamma_2 \delta Y_0$ and $\delta Y_1^1 = (\mathrm{e}^{\mathcal{M}\Delta} + q_2\gamma_2)\delta Y_0$. Eq. (95) has the same form as Eq. (48), so that the stability of the synchronous network state follows from the same argument as the stability of the period one orbit for a single neuron. Even more so, since the matrix B_N seems to always possess an eigenvalue equal to one as does the matrix B in Eq. (48). Below a critical value, at least one eigenvalue has a modulus larger than one, indicating that the synchronous network state is unstable. This

is confirmed by direct numerical solutions which show that below the instability point neurons oscillate with a clear phase lag. On the contrary, increasing the coupling strength g stabilises the synchronous network state.

The linear stability analysis that we presented in Section 5 for a single neuron focused on positive voltages with the effect that the dynamics is described by one matrix $M = A_1$ only. In turn, this allowed us to write down a single governing equation for all times and to relate the perturbations at the nth firing event to the previous one through M alone. However, the model also supports period one orbits where the reset takes the voltage to negative values (regular spiking). In this case, we need to consider two matrices to capture the behavior of the neuron. The linear stability analysis for such a large amplitude oscillation can be achieved by combining the present results with those of an earlier study [65], which demonstrates the linear stability analysis for a PWL system with multiple switching events along a period one orbit. While we here investigate state-dependent switching, i.e. the discontinuity occurs if a given variable reaches a threshold value, applying ideas from [65] also provides a handle on time-dependent switches. In turn, this allows us to study nonsmooth PWL systems with an arbitrary sequence of state- and time-dependent switching events.

Although we illustrated the linear stability analysis of a synchronous network state in a network of two neurons only, this holds all the ingredients to study larger networks. Firstly, it is reasonable to assume that all neurons reach threshold between consecutive firings of a given neuron because we perturb around the synchronous network state where all neurons fire at the same time. Hence, there are N perturbations around the same firing time T_n and hence $(N-1)$ iterations of the steps that lead to Eq. (80) instead of only one. Secondly, the same arguments that result in Eq. (88) need to be considered in a network, since there once all of the neurons have reached threshold around some T_n, the next firing event in the network will occur around T_{n+1}. It is worth pointing out that our analysis of the synchronous network state holds for arbitrary network topologies and an arbitrary number of components of a single neuron through which the coupling occurs. All this information is encoded in the matrices G and H, which are kept general throughout the analysis. Moreover, the analysis works for any coupling strength. One caveat of the approach presented here is that the order in which the neurons fire has to be prescribed, so that we need to restrict our attention to specific classes of network perturbations. However, at least in globally connected networks where all neurons are identical, such an order can be assigned naturally.

8.2. Asynchronous states

Here we shall focus on asynchronous states defined by $\phi_\alpha = \alpha/N$. Such solutions are often called splay or merry-go-round states, since all oscillators in the network pass through some fixed phase at regularly spaced time intervals of Δ/N. Moreover, we shall consider a globally coupled network in the large N limit. Of all possible phase locked-states in a network these so-called asynchronous states are in some sense, as quantified by a synchrony measure like that of [66], farthest from synchrony. In the large N limit we have the useful result that network averages may be replaced by time averages and the coupling term for an asynchronous state becomes

$$\lim_{N\to\infty}\frac{1}{N}\sum_{\beta=1}^{N} v(t+\beta\Delta/N)=\frac{1}{\Delta}\int_0^\Delta v(t)\mathrm{d}t, \tag{96}$$

which is independent of both α and t (assuming $v(t)$ is continuous for $t\in[0,\Delta)$). Hence, for an asynchronous state every neuron in the network is described by the same dynamical system, namely

$$\dot v = f(v)-gv+I-a+gv_0, \qquad \dot a=\omega(\beta v-a), \tag{97}$$

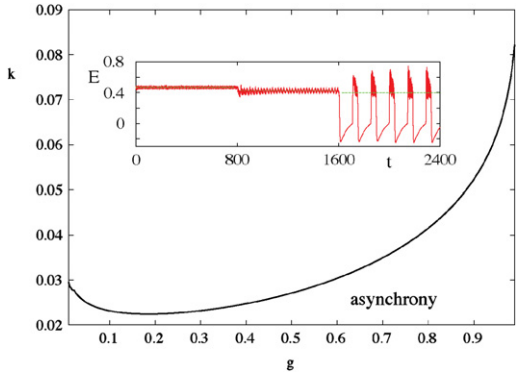

Fig. 17. Curve showing the bifurcation defined by Re $\lambda = 0$ and Im $\lambda \neq 0$. Parameter values are $\beta = 0, \omega = 1/75$ and $I = 0.1$. Beyond an instability point of the asynchronous solution one typically sees the emergence of synchronised bursting states, as shown in the inset. Inset: A plot showing an instability of the asynchronous state in a network with $N = 100$ neurons, starting from a randomly perturbed splay state. The solid line is the value of the mean-field signal $E(t) = N^{-1}\sum_{\alpha=1}^{N} v^\alpha(t)$, and the dashed line is the analytically calculated value for the mean field signal v_0 for the asynchronous state. At $t = 800$ the value of k is switched from $k = 0.02$ (where the asynchronous state is stable) to $k = 0.028$ (just beyond the border of stability) and at $t = 1600$ it is switched again to $k = 0.03$. This nicely illustrates that as one moves through the stability border that periodic variations in the mean-field signal can emerge and ultimately lead to a synchronised bursting state. Parameters are $\beta = 0, \omega = 1/75$, $v_R = 0.2$, $v_{th} = 1$, $I = 0.1$ and $g = 0.5$.

where

$$v_0=\frac{1}{\Delta}\int_0^\Delta v(t)\mathrm{d}t. \tag{98}$$

The asynchronous state can then be found as a Δ-periodic solution of (97), which can either be done numerically (using a boundary value solver as described in Appendix D of [7]) for a general choice of f or analytically for the PWL-IF model [32]. The stability of this state can also be determined using a phase-density technique, first developed by van Vreeswijk [67] for synaptic coupling and later extended by Coombes to treat electrical coupling [7,32]. The eigenvalues determining stability are given as the zeros of the function $\mathcal{E}(\lambda)$, where

$$\mathcal{E}(\lambda)=\frac{\mathrm{e}^{\lambda\Delta}}{\widetilde v(\lambda)}-g\lambda\Delta\int_0^1\Gamma(\theta\Delta)\mathrm{e}^{\lambda\theta\Delta}\mathrm{d}\theta. \tag{99}$$

Here Γ is the g-dependent voltage component of the adjoint for the asynchronous state (that has to be determined from (97)) and $\widetilde v(\lambda)$ is the Laplace transform of the known periodic orbit $v(t)$. The asynchronous state is stable if Re$\lambda < 0$. The proof of the stability condition is given in [7].

We illustrate the use of this stability analysis by applying it to a fast spiking orbit with $\beta = 0$. Using the above construction we find that for fixed g and increasing k a pair of complex conjugate eigenvalues crosses through the imaginary axis (away from zero). This signals the onset of a dynamic instability. Because the underlying model is described by a discontinuous flow then there is also the possibility that a nonsmooth bifurcation can occur. For the parameters considered here we find that a dynamic instability of the splay state is always met before the onset of a nonsmooth bifurcation [32]. By tracking the bifurcation point Re $\lambda = 0$ in parameter space it is possible to map out those regions where the asynchronous state is stable. We do this in Fig. 17 which shows that if an asynchronous state is stable for fixed g or I then it can always be destabilised by increasing k beyond some critical value.

To determine the types of solutions that emerge beyond the instability borders we have performed direct numerical simulations. Not only do these confirm the correctness of our bifurcation theory,

they show that a dominant emergent solution is a bursting mode in which neurons are synchronised at the level of their firing rates, but not at the level of individual spikes (within a burst). An example of a network state that switches from asynchronous tonic spiking to synchronised bursting with a switch in k across the bifurcation point is shown in the inset of Fig. 17. Here we plot the mean field signal $E(t) = N^{-1}\sum_{\alpha=1}^{N} v^{\alpha}(t)$ for a network of $N = 100$ neurons.

9. Discussion

In this paper we have provided an overview of nonlinear IF models that are currently of interest to the computational neuroscience community. Their obvious discontinuous nature means that much can be gained from mathematical studies that make use of the growing variety of tools and techniques being developed for the study of nonsmooth systems. By introducing a particular form of PWL IF model in this paper we have shown that the time is ripe for the study of not only singe neuron dynamics, but also networks. Single neuron studies in response to natural stimuli are highly relevant for understanding sensory processing and unravelling the neural code, whilst theoretical analysis of large scale spiking networks is relevant to brain studies at the highest level, and in particular for neural computation and cognition.

It is worth mentioning a number of explicit next steps for the mathematical neuroscience community, that can build upon some of the ideas we have presented here. The construction of Arnol'd tongues for more general nonlinear IF models and in particular the PWL-IF model is one obvious next step, generalising the approach used for the LIF model. Indeed, developing a way to describe the response of such models to more complicated signals than just periodic ones is also vital for understanding how neurons process natural stimuli. At the network level it is quite common to first consider the behaviour of a set of weakly interacting oscillators, where knowledge of the PRC is key to making progress. We have shown how to do this here for the PWL-IF model (and indeed it is straightforward to do this for any single variable nonlinear IF model). However, we did not discuss the notion of isochronal coordinates that underpins the usefulness of a coupled oscillator theory. Indeed to understand the response of spiking neurons to perturbation it would be very useful to construct isochrons (which in the context of smooth dynamical systems can be interpreted as leaves of the stable manifold of a hyperbolic limit cycle). Techniques for doing this may well generalise from those used in smooth systems, such as in [68,69], and it would be interesting to pursue this further. At the network level we presented examples of phase-locked states in linearly coupled systems. Although this is highly relevant to electrical gap junction coupling it does not describe chemical synaptic coupling. In this case it is natural to consider event based coupling, as in [20], and it then remains a challenge to develop a theory of strong interactions. Once again focusing on models with a sub-threshold PWL dynamics may allow for progress. Moreover, it is a challenge to develop the notion of Lyapunov exponents for such networks, although progress in this direction has recently been made for discrete-time LIF systems [70].

For a further discussion of the role of mathematics in neuroscience and other outstanding challenges we refer the reader to [71] and to the aims and scopes of the newly established Journal of Mathematical Neuroscience at http://www.mathematical-neuroscience.com/.

Acknowledgments

We would like to thank Magnus Richardson and Laurent Badel for interesting discussions regarding the use of IF models in neuroscience as well as providing Fig. 3. RT was supported by the Leverhulme Trust through an Early Career Fellowship.

References

[1] H. Markram, The blue brain project, Nat. Rev. Neurosci. 7 (2006) 153–160.
[2] R. Fitzhugh, Impulses and physiological states in theoretical models of nerve membranes, Biophys. J. 1182 (1961) 445–466.
[3] H.P. McKean, Nagumo's Equation, in: Advances in Mathematics, vol. 4, 1970, pp. 209–223.
[4] W.P. Wang, Multiple impulse solutions to McKean's caricature of the nerve equation. I. Existence, Comm. Pure Appl. Math. 41 (1988) 71–103.
[5] W.P. Wang, Multiple impulse solutions to McKean's caricature of the nerve equation. II. Stability, Comm. Pure Appl. Math. 41 (1988) 997–1025.
[6] A. Tonnelier, The McKean's caricature of the FitzHugh–Nagumo model I. The space-clamped system, SIAM J. Appl. Meth. 63 (2002) 459–484.
[7] S. Coombes, Neuronal networks with gap junctions: a study of piece-wise linear planar neuron models, SIAM J. Appl. Dyn. Syst. 7 (2008) 1101–1129.
[8] H.G. Rotstein, S. Coombes, A.-M. Gheorghe, Canard-like explosion of limit cycles in two-dimensional piecewise-linear models of FitzHugh–Nagumo type, SIAM J. Appl. Dyn. Syst. (under revision).
[9] E.M. Izhikevich, G.M. Edelman, Large-scale model of mammalian thalamocortical systems, Proc. Natl. Acad. Sci. 105 (2008) 3593–3598.
[10] S.J. Hogan, On the dynamics of rigid-block motion under harmonic forcing, Proc. R. Soc. Lond. Ser. A 425 (1989) 441–476.
[11] A. Kaharaman, R. Singh, Nonlinear dynamics of a spur gear pair, J. Sound Vib. 142 (1990) 49–75.
[12] P.C. Tung, S.W. Shaw, A method for the improvement of impact printer and performance, Trans. ASME, J. Vib. Acoust. Stress Reliab. Des. 110 (1998) 528–532.
[13] M. di Bernardo, C. Budd, A.R. Champneys, P. Kowalczyk, Piecewise-Smooth Dynamical Systems: Theory and Applications, Springer, 2007.
[14] M. di Bernardo, C.J. Budd, A.R. Champneys, P. Kowalczyk, A.B. Nordmark, G.O. Tost, P.T. Piiroinen, Bifurcations in nonsmooth dynamical systems, SIAM Rev. 50 (2008) 629–701.
[15] A.L. Hodgkin, A.F. Huxley, A quantitative description of membrane current and its application to conduction and excitation in nerve tissue, J. Physiol. (London) 116 (1952) 449–472.
[16] L. Badel, S. Lefort, T.K. Berger, C.C.H. Petersen, W. Gerstner, M.J.E. Richardson, Extracting nonlinear integrate-and-fire models from experimental data using dynamic I–V curves, Biol. Cybernet. 99 (2008) 361–370.
[17] W. Gerstner, W. Kistler, Spiking Neuron Models, Cambridge University Press, 2002.
[18] J. Platkiewicz, R. Brette, A threshold equation for action potential initiation, PLoS Comput. Biol. 6 (2010) e1000850.
[19] N. Brunel, M.C.W. van Rossum, Lapicque's 1907 paper: from frogs to integrate-and-fire, Biol. Cybernet. 97 (2007) 337–339.
[20] P.C. Bressloff, S. Coombes, Dynamics of strongly coupled spiking neurons, Neural Comput. 12 (2000) 91–129.
[21] P.E. Latham, B.J. Richmond, P.G. Nelson, S. Nirenberg, Intrinsic dynamics in neuronal networks I. Theory, J. Neurophysiol. 83 (2000) 808–827.
[22] E.M. Izhikevich, Dynamical Systems in Neuroscience: The Geometry of Excitability and Bursting, The MIT Press, 2007.
[23] N. Fourcaud-Trocme, D. Hansel, C. van Vreeswijk, N. Brunel, How spike generation mechanisms determine the neuronal response to fluctuating inputs, J. Neurosci. 23 (2003) 11628–11640.
[24] E.M. Izhikevich, Simple model of spiking neurons, IEEE Trans. Neural Netw. 14 (2003) 1569–1572.
[25] E.M. Izhikevich, Hybrid spiking models, Philos. Trans. R. Soc. Lond. Ser. A 368 (2010) 5061–5070.
[26] J. Touboul, Importance of the cutoff value in the quadratic adaptive integrate-and-fire model, Neural Comput. 21 (2009) 2114–2122.
[27] T. Gröbler, G. Barna, P. Érdi, Statistical model of the hippocampal CA3 region I. The single-cell module: bursting model of the pyramidal cell, Biol. Cybernet. 79 (1998) 301–308.
[28] R. Brette, W. Gerstner, Adaptive exponential integrate-and-fire model as an effective description of neuronal activity, J. Neurophysiol. 94 (2005) 3637–3642.
[29] J. Touboul, R. Brette, Dynamics and bifurcations of the adaptive exponential integrate-and-fire model, Biol. Cybernet. 99 (2008) 319–334.
[30] J. Touboul, Bifurcation analysis of a general class of nonlinear integrate-and-fire neurons, SIAM J. Appl. Meth. 68 (2008) 1045–1079.
[31] J. Karbowski, N. Kopell, Multispikes and synchronization in a large-scale neural network with delays, Neural Comput. 12 (2000) 1573–1606.
[32] S. Coombes, M. Zachariou, Coherent Behavior in Neuronal Networks, in: Springer Series in Computational Neuroscience, vol. 3, Springer, 2009 pp. 77–94. (Chapter) Gap junctions and emergent rhythms.
[33] P.L. Boyland, Bifurcations of circle maps: Arnol'd tongues, bistability and rotation intervals, Comm. Math. Phys. 106 (1986) 353–381.
[34] J.P. Keener, F.C. Hoppensteadt, J. Rinzel, Integrate-and-fire models of nerve membrane response to oscillatory input, SIAM J. Appl. Math. 41 (3) (1981) 816–823.
[35] S. Coombes, P.C. Bressloff, Mode-locking and Arnold tongues in integrate-and-fire neural oscillators, Phys. Rev. E 60 (1999) 2086–2096.
[36] S. Coombes, P.C. Bressloff, Erratum: mode-locking and Arnold tongues in integrate-and-fire neural oscillators, Phys. Rev. E 63 (2001) 059901.
[37] J. Laudanski, S. Coombes, A.R. Palmer, C.J. Sumner, Mode-locked spike trains in responses of ventral cochlear nucleus chopper and onset neurons to periodic stimuli, J. Neurophysiol. 103 (2010) 1226–1237.
[38] S. Coombes, R. Thul, J. Laudanski, A.R. Palmer, C.J. Sumner, Neuronal spike-train responses in the presence of threshold noise, Front. Life Sci. (in press).

[39] Y. Ono, K. Aihara, H. Suzuki, Grazing bifurcation and mode-locking in reconstructing chaotic dynamics with a leaky integrate-and-fire model, Artif. Life Robot. 7 (2003) 55–62.
[40] S. Coombes, M.R. Owen, G.D. Smith, Mode-locking in a periodically forced integrate-and-fire-or-burst neuron model, Phys. Rev. E 64 (2001) 041914.
[41] C.R. Laing, S. Coombes, Mode locking in a periodically forced "Ghostbursting" neuron model, Internat. J. Bifur. Chaos 15 (2005) 1433–1444.
[42] A.K. Alijani, Mode locking in a periodically forced resonate-and-fire neuron model, Phys. Rev. E 80 (2009) 051922(1–12).
[43] C.-M. Svensson, S. Coombes, Mode locking in a spatially extended neuron model: active soma and compartmental tree, Internat. J. Bifur. Chaos 19 (2009) 2597–2607.
[44] J. Laudanski, C.J. Sumner, S. Coombes, Calcium window currents, periodic forcing and chaos: understanding single neuron response with a discontinuous one dimensional map, Phys. Rev. E 82 (2010) 011924(1–9).
[45] A.B. Nordmark, Universal limit mapping in grazing bifurcations, Phys. Rev. E 55 (1997) 266–270.
[46] A. Tonnelier, W. Gerstner, Piecewise linear differential equations and integrate-and-fire neurons: insights from two-dimensional membrane models, Phys. Rev. E 67 (2003) 021908(1–16).
[47] D. Simpson, J. Meiss, Andronov–Hopf bifurcations in planar, piecewise-smooth, continuous flows, Phys. Lett. A 371 (2007) 213–220.
[48] G.B. Ermentrout, D. Terman, Foundations of Mathematical Neuroscience, Springer, 2010.
[49] E. Brown, J. Moehlis, P. Holmes, On the phase reduction and response dynamics of neural oscillator populations, Neural Comput. 16 (2004) 673–715.
[50] B. Ermentrout, Simulating, Analyzing, and Animating Dynamical Systems: A Guide to Xppaut for Researchers and Students, Society for Industrial & Applied Mathematics, 2002.
[51] Y. Kuramoto, Chemical Oscillations, Waves and Turbulence, Springer-Verlag, 1984.
[52] J. Touboul, R. Brette, Spiking dynamics of bidimensional integrate-and-fire neurons, SIAM J. Appl. Dyn. Syst. 8 (2009) 1462–1506.
[53] G.S. Medvedev, Reduction of a model of an excitable cell to a one-dimensional map, Physica D 202 (2005) 37–59.
[54] T.R. Chay, J. Keizer, Minimal model for membrane oscillations in the pancreatic beta-cell, Biophys. J. 42 (1983) 181–190.
[55] R. Bertram, A. Sherman, Bursting: The Genesis of Rhythm in the Nervous System, World Scientific, 2005, (Chapter) Negative calcium feedback: the road from Chay–Keizer, pp. 19–48.
[56] H. Marotto, Snap-back repellers imply chaos in $\mathbb{R}^n$, J. Math. Anal. Appl. 63 (1978) 199–223.
[57] G. Zheng, A. Tonnelier, Chaotic solutions in the quadratic integrate-and-fire neuron with adaptation, Cogn. Neurodyn. 3 (2009) 197–204.
[58] P.C. Müller, Calculation of Lyapunov exponents for dynamic-systems with discontinuities, Chaos Solitons Fractals 5 (9) (1995) 1671–1681.
[59] M. Galarreta, S. Hestrin, A network of fast-spiking cells in the neocortex connected by electrical synapses, Nature 402 (1999) 72–75.
[60] B.W. Connors, M.A. Long, Electrical synapses in the mammalian brain, Annu. Rev. Neurosci. 27 (2004) 393–418.
[61] F.O. Schmitt, P. Dev, B.H. Smith, Electronic processing of information by brain cells, Science 193 (1976) 114–120.
[62] S.G. Hormuzdi, M.A. Filippov, G. Mitropoulou, H. Monyer, R. Bruzzone, Electrical synapses: a dynamic signaling system that shapes the activity of neuronal networks, Biochim. Biophys. Acta 1662 (2004) 113–137.
[63] J.L.P. Velazquez, P.L. Carlen, Gap junctions, synchrony and seizures, Trends Neurosci. 23 (2000) 68–74.
[64] P. Ashwin, J.W. Swift, The dynamics of n weakly coupled identical oscillators, J. Nonlinear Sci. 2 (1992) 69–108.
[65] R. Thul, S. Coombes, Understanding cardiac alternans: a piecewise linear modelling framework, Chaos 20 (2010) 045102.
[66] P.F. Pinsky, J. Rinzel, Synchrony measures for biological neural networks, Biol. Cybernet. 73 (2) (1995) 129–137.
[67] C. van Vreeswijk, Analysis of the asynchronous state in networks of strongly coupled oscillators, Phys. Rev. Lett. 84 (2000) 5110–5113.
[68] A. Guillamon, G. Huguet, A computational and geometric approach to phase resetting curves and surfaces, SIAM J. Appl. Dyn. Syst. 8 (2009) 1005–1042.
[69] H.M. Osinga, J. Moehlis, Continuation-based computation of global isochrons, SIAM J. Appl. Dyn. Syst. 9 (2010) 1201–1228.
[70] B. Cessac, T. Viéville, On dynamics of integrate-and-fire neural networks with conductance based synapses, Front. Comput. Neurosci. 2 (2008) doi:10.3389/neuro.10.002.2008.
[71] S. Coombes, Mathematical neuroscience, J. Math. Biol. 54 (2007) 305–307.